NOAA OAR Special Report

PMEL Tsunami Forecast Series: Vol. 12

A Tsunami Forecast Model for Mayagüez, Puerto Rico

Burak Uslu [1,2]

[1]Joint Institute for the Study of the Atmosphere and Ocean (JISAO), University of Washington, Seattle, WA

[2]NOAA/Pacific Marine Environmental Laboratory (PMEL), Seattle, WA

August 23, 2013

NOTICE from NOAA

Mention of a commercial company or product does not constitute an endorsement by NOAA/OAR. Use of information from this publication concerning proprietary products or the tests of such products for publicity or advertising purposes is not authorized. Any opinions, findings, and conclusions or recommendations expressed in this material are those of the authors and do not necessarily reflect the views of the National Oceanic and Atmospheric Administration.

Contribution No. 3353 from NOAA/Pacific Marine Environmental Laboratory
Contribution No. 1774 from Joint Institute for the Study of the Atmosphere and Ocean (JISAO)

Also available from the National Technical Information Service (NTIS)
(http://www.ntis.gov)

Contents

List of Figures

List of Tables

Foreword

Tsunamis have been recognized as a potential hazard to United States coastal communities since the mid-twentieth century, when multiple destructive tsunamis caused damage to the states of Hawaii, Alaska, California, Oregon, and Washington. In response to these events, the United States, under the auspices of the National Oceanic and Atmospheric Administration (NOAA), established the Pacific and Alaska Tsunami Warning Centers, dedicated to protecting United States interests from the threat posed by tsunamis. NOAA also created a tsunami research program at the Pacific Marine Environmental Laboratory (PMEL) to develop improved warning products.

The scale of destruction and unprecedented loss of life following the December 2004 Sumatra tsunami served as the catalyst to refocus efforts in the United States on reducing tsunami vulnerability of coastal communities, and on 20 December 2006, the United States Congress passed the "Tsunami Warning and Education Act" under which education and warning activities were thereafter specified and mandated. A "tsunami forecasting capability based on models and measurements, including tsunami inundation models and maps..." is a central component for the protection of United States coastlines from the threat posed by tsunamis. The forecasting capability for each community described in the PMEL Tsunami Forecast Series is the result of collaboration between the National Oceanic and Atmospheric Administration office of Oceanic and Atmospheric Research, National Weather Service, National Ocean Service, National Environmental Satellite, Data, and Information Service, the University of Washington's Joint Institute for the Study of the Atmosphere and Ocean, National Science Foundation, and United States Geological Survey.

NOAA Center for Tsunami Research

Abstract

The National Oceanic and Atmospheric Administration has developed a tsunami forecast model for Mayagüez, Puerto Rico as part of the Tsunami Warning and Education Act. This study describes the development, validation, and stability tests of the model designed for Mayagüez, Puerto Rico. The forecast model development process includes compilation of bathymetric and topographic data and creation of higher-resolution reference model grids, and optimezed resolution forecast model grids capable of producing an inundation forecast in minutes. Mayagüez Model is tested for the 1755 Lisbon and 1918 Mona Passage historical tsunamis as well as seven synthetic scenarios. Results shows that the designed forecast model will be successfully used in predicting tsunami hazard operationally and tsunamis generated from the Muertos Trough and the Puerto Rico Trench pose the largest threat to Mayagüez.

Chapter 1

Background and Objectives

The National Oceanic and Atmospheric Administration (NOAA) Center for Tsunami, Research (NCTR) at the NOAA Pacific Marine Environmental Laboratory (PMEL) has developed a tsunami forecasting capability for operational use by NOAA's two Tsunami Warning Centers located in Hawaii and Alaska (Titov et al., 2005). The system is designed to efficiently provide basin-wide warning of approaching tsunami waves accurately and quickly. Forecast models provided combines real-time tsunami event data with numerical models to produce estimates of tsunami wave arrival times and amplitudes at a coastal community of interest.

The primary goal of the system termed Short-term Inundation Forecast of Tsunamis (SIFT) is to provide NOAA Tsunami Warning Centers with operational tools that combine real-time deep-ocean Bottom Pressure Recorder (BPR) recordings from the tsunameter network (Eble and González, 0401) and seismic data with a suite of numerical codes, and the Method of Splitting Tsunami (MOST) (Titov and Synolakis, 1998; Titov and González, 1997), to produce efficient forecasts of tsunami arrival time, height, and inundation. To achieve accurate and detailed information on the likely impact of incoming tsunamis on specific coastal communities within certain time limits and to reduce false alarms, 75 forecast models are being developed and integrated as components of SIFT for a limited number of 75 U.S. coastal cities and territories that are potentially at most risk.

The present study reports development and testing of forecast models for the city of Mayagüez on the island of Puerto Rico. Figure 1 shows the Caribbean Sea and the island of Puerto Rico. In a more detailed Figure 2, Puerto Rico coastlines is shown with capital San Juan in the north, Ponce in the south and Mayagüez located in the west coast of the island. Details and procedures in development of this forecast model is outlined in Synolakis et al. (2008) and Tang et al. (2009).

1.1 Puerto Rico History

First European arrival in the Puerto Rico was by Christopher Columbus in 1493, who named the island San Juan Bautista, which eventually became the name of the capital of the island. Followed by this exploration, the island was colonized by Spain and named as the "rich port" or "Puerto Rico" because of the gold found in its rivers (Smithsonian Magazine, 2013).

Indigenous Taíno and Carib races were mixed with Spanish and African immigrants dur-

ing Spanish colonization from 1493 until 1898. Many indigenous town names are still in use, such as Mayagüez and Utuado (Figure 2). Puerto Rico was a secure Spanish port, even though numerous assaults were attempted by French, Dutch and British. Finally, United States forces invaded Puerto Rico following the Spanish-American war, and the island was ceded to United States by the 1898 Treaty of Paris (Smithsonian Magazine, 2013).

In 1917 Puerto Ricans were granted full U.S. Citizenship and in the mid 1900s the island's economy flourished by the industrialization effort called Operation Bootstrap, which provided cheap labor and tax-aid for the American companies. Puerto Rican economy flourished and still relies on manufacturing and tourism, where Puerto Rico provides high-tech equipments and pharmaceuticals goods to United States. Puerto Rico became part of U.S. Commonwealth in 1952 adopting the U.S. constitution (History.com, 2013). From World War II until 2003, two thirds of the island had been purchased and occupied by the U.S. Navy for military practices. Due to an accident occurred in 2003, the Navy had to evacuate and the Navy land has been designated to a wild life reserve.

1.2 Tide Station

Hence, the economical importance and the major base in Caribbean, a forecasting capability for Puerto Rico is necessary and Mayagüez forecast model is prepared as outlined in this study. Figures 2 and 3 shows the town of Mayagüez and the location of the tide station in Mayagüez Harbor. Tide stations are usually designated as the warning point and tsunami warning centers rely their warnings depending on the predicted wave amplitude at these locations. Location of the station in Mayagüez, which is part of the Puerto Rico Seismic Network (Vélez-Rodríguez, 2007a), is shown in Figure 3 provided by Vélez-Rodríguez (2007a), as well as the illustration by Vélez-Rodríguez (2007b). Location of the station is marked on a satellite image in the Figure 3, courtesy of Google Earth. In the forecast model and reference model, the nearest wet point is selected as the synthetic tide gauge node representing the predictions for the tide station. Depth of water in the numerical models for tide station is 0.7 m.

1.3 Tsunamis in Puerto Rico

Tsunamis in Caribbean are not as frequent as they are in Pacific Ocean, however, active fault lines around the region has helped tsunamis observed from variety of sources including trans-oceanic earthquake, volcanic eruptions and submarine landslides.

O'Loughlin and Lander (2003) reports two trans-oceanic tsunamis observed in the Caribbean generated in Europe, as early as in 16th century. The 1755 Lisbon tsunami that had inundation in the Lesser Antilles and the 1761 Iberian tsunami that was observed with a 1.2m run-up height in Barbados (Lander and Whiteside, 2007; O'Loughlin and Lander, 2003; Baptista et al., 1998, 2003)

Caribbean also has a history of local tsunamis as well. In 1918 a M_L 7.5 earthquake in the Mona Passage between Hispaniola and Puerto Rico (Figure 1) triggered a tsunami that affected mostly western coast of Puerto Rico and causing more than 100 casualties. Lopez-Venegas et al. (2008) study discusses the geologic evidence of a large scale submarine landslide that is related to the source of the 1918 tsunami. A run-up of 1.1-1.5 m wave was observed in Mayagüez 25-30

minutes after the earthquake.

National Geophysical Data (2013) holds the most current up to date database of tsunami observations in the world. Harbitz et al. (2012) studied tsunami hazards in the Caribbean looking at tsunami sources from landslide, volcanic eruptions and earthquakes. Harbitz et al. (2012) holds a very valuable and detailed database of historical tsunamis in the Caribbean and lists the M_S 7.5 Virgin Islands earthquake as the sources of highest tsunamis of Caribbean. The run-up height has been debated between 18.3 m and 10 m. Historical investigation of documentation and surveys are discussed by Zahibo and Pelinovsky (2001); Zahibo et al. (2003) and numerical modeling of this event has been performed by Zahibo et al. (2008); Harbitz et al. (2012); Barkan and ten Brink (2010).

In this study, the 1755 Lisbon and 1918 Mona Passage tsunamis are modeled. Computed wave amplitudes are compared to historical accounts.

Chapter 2

Forecast Methodology

Two complete sets of grids were developed from NOAA's National Geophysical Data Center high resolution bathymetric database (Taylor et al., 2007) . Aim for the first set is to provide the best available solution from the most up to date elevation model. High resolution grids are referred to as reference grid models and they are designed for research purposes to provide the most accurate prediction of wave amplitudes, wave arrival time and currents in Mayagüez, Puerto Rico. Second set of grids are optimized from the reference model to provide computation with in time constrains and yet to be accurate enough for warning purposes. All forecast models are compare with reference model test scenarios for their predictions.

In general a tsunami forecast model is a set of high-resolution grids constructed by the Pacific Marine Environmental Laboratory, that computes and provides a tsunami inundation for a selected coastal community in real-time within minutes of an earthquake. The Method of Splitting Tsunami (MOST) is a suite of numerical simulation codes capable of simulating three processes of tsunami evolution: earthquake, transoceanic propagation, and inundation of dry land. The MOST model has been extensively tested against a number of laboratory experiments and benchmarks (Synolakis et al., 2008) and was successfully used for simulations of many historical tsunami events. The main objective of a forecast model is to provide an accurate, yet rapid, estimate of wave arrival time, wave height, and inundation in the minutes following a tsunami event. Titov and González (1997) describe the technical aspects of forecast model development, stability, testing, and robustness, and Tang et al. (2009).

A basin-wide database of pre-computed water elevations and flow velocities for unit sources covering worldwide subduction zones has been generated to expedite forecasts (Gica et al., 2008). As the tsunami wave propagates across the ocean and successively reaches tsunameter observation sites, recorded sea level is ingested into the tsunami forecast application in near real-time and incorporated into an inversion algorithm to produce an improved estimate of the tsunami source. A linear combination of the pre-computed database is then performed based on this tsunami source, a source that reflects the transfer of energy to the fluid body and thus a transfer of the governing physics from earth to ocean, to produce synthetic boundary conditions of water elevation and flow velocities to initiate the forecast model computation.

Accurate forecasting of the tsunami impact on the target forecast area largely relies on the accuracies of bathymetry and topography and the numerical computation. The spatial and temporal grid resolution necessary for modeling accuracy poses a challenge in the run-time requirement for real-time forecasts. Each forecast model consists of three telescoped grids with

increasing spatial resolution in the finest grid, and temporal resolution for simulation of wave inundation onto dry land. The forecast model utilizes the most recent bathymetry and topography available to reproduce the correct wave dynamics during the inundation computation. Previous and present development of forecast models in the Pacific and Atlantic Ocean((Titov et al., 2005; Titov, 2009; Wei et al., 2008; Tang et al., 2008b) have been validated for the accuracy and efficiency. Models are tested in real-time at every opportunity during an event and they are used for scientific research, as well. Tang et al. (2009) provide forecast model development methodology details.

Metropolitan population of Mayagüez is 106,330 is according to U.S. Census Bureau (2012), making it an important port town. Mayagüez, unlike the port towns in Pacific Ocean, does not have a very high relief. The deepest point in the grid modeled for harbor is 171 m and that is approximately seven kilometers off shore. Highest point in the same grid is 259 m.

Mayaguez is located on the West of Puerto Rico in North East Caribbean. Location of Puerto Rico relative to the Caribbean Sea is shown in Figure 1, where it is approximately 140 km East of Dominican Republic and 750 East of Cuba. Florida is the southern most state in continental United States, which is approximately a 1600 km flight distance from Miami, FL to Mayagüez, PR. Caribbean islands are results of the interactions between North American plate and Caribbean Sea. Geological setting of fault lines surrounding Puerto Rico is shown in Figure 1. Puerto Rico is an uplif result of submergence of Hispaniola and Puerto Rico Trenches in the North and Muertos Trough in the South (Granja Bruña et al., 2009).

Chapter 3

Model Development

The Mayagüez forecast model is developed from high-resolution digital elevation model was provided by NOAA's National Geophysical Data Center (NGDC). High-resolution grids for the Mayagüez and its vicinity are constructed from the best available data source shown in Figure 4. A Forecast Model is an optimized version of a reference high resolution model, where a forecast model has to compute results in a time constrain operational restrictions, yet their results has to agree with a reference model. Reference Model are produced at Pacific Marine and Environmental Laboratories for research purposes and they are used in purposes that forecast models are not sufficient, such as hazard assessments and studies tsunami currents in the ports (Uslu et al., 2013, 2010b,a). Forecast models reduced in resolution and details, but they are designed to provide reliable predictions that agrees with reference models for warning centers.

Referred to as A, B, and C, the three nested grids each become successively finer in resolution as they telescope into study area. The largest coverage is from the lowest resolution A-grid that extends from offshore Puerto Rico to deep ocean, while the near-shore details are resolved within the finest scale C-grid to the point that tide gauge observations recorded during historical tsunamis are resolved within expected accuracy limits. The general procedure to develop the forecast model is to begin development with large spatial extent merged bathymetric topographic grids at high resolution, and then optimize these grids by sub sampling to coarsen the resolution and shrink the overall grid dimensions to achieve a 4 to 10 hr simulation of modeled tsunami waves within the required time period of 10 min of wall-clock time. The forecast model is developed by incrementally reducing the resolution and extent of the coverage of the reference model, as described in (Tang et al., 2008a). It is possible to develop 3 arc-sec fast-running optimized numerical grids that can predict time histories at desired numerical tide gauges with high accuracy (Tang et al., 2006).

3.1 Source digital elevation models

The National Geophysical Data Center (NGDC) developed the digital elevation models for Puerto Rico using numerous source of bathymetric, topographic and shoreline data from federal, state government agencies and universities. Data from the U.S. Geological Survey (USGS); the NOAA National Ocean Service (NOS), National Geodetic Survey (NGS), Office of Coast Survey (OCS)

and National Centers for Coastal Ocean Science (NCOOS); the Puerto Rico Planning Board (PRPB); the Puerto Rico Office of Management and Budget; and the University of Puerto Rico are processed and combined with the procedures described in Taylor et al. (2007) for relative to local Mean High Water as the vertical datum and World Geodetic System 1984 as the horizontal datum. Figure 4 shows the source of datasets used in compiling of Puerto Rico digital elevation model, primarily from NOS hydrographic and LIDAR surveys, U.S. Army Corps of Engineers Scanning Hydrographic Operational Airborne Lidar Surveys (SHOALS) , and a deep water multibeam sonar surveys collected by the U.S. Geological Survey.

3.2 Reference model grids

A set of three nested high-resolution model grids were created (Figure 4) from the source digital elevation model provided by NGDC (Taylor et al., 2007) described in previous section. These reference grids provide guidance for the development of optimized forecast grids of lower resolution and smaller extent that will allow the model to operate in real time (Tang et al., 2009). Figure 5 shows and Table 2 lists the setup parameters and details of the the reference model. Optimized grids designed in this report were all tested against the reference model for reliability and stability. Three nested grids, referred to as A, B, and C-grids, each of which becomes successively finer in resolution as they telescope into the population and economic center of the community of interest. The offshore area is covered by the largest and lowest 24 arc-sec resolution A grid that extends from continental shelf of Caribbean Sea to Atlantic Ocean. B grid with 6 arc-sec resolution covers the entire Puerto Rico and the Mayagüez is modeled with 1 arc-sec for detailed computations. A discrepancy in the A grid is visible in the reference model in the East of Puerto Rico. This issue is addressed in the forecast model and for future study for hazard assessment reference model will need to be updated.

3.3 Forecast model grids

Forecast models are designed by using subsamples of the reference model or optimized grids from the source digital elevation model from NGDC. In total six grids are developed and five combination of these grids are test in this study. One of them is designated for the use for the NOAA tsunami warning system predictions. Details of the forecast models are listed in Table 1 and extends of these are shown in Figure 6.

The forecast model is required to produce wave height and inundation forecasts that agrees with the reference model. All five forecast model computed simulations for 10 hours of wave propagation. Models are named S1, S2, S3, S4, and S5 in the Table 1 respectively, and CPU time for each model ranges from 9 minutes to 25 minutes. Two different A Grids, two B Grids and two C Grids are used in five sets of combination in this study. S1 has the highest resolution and the largest coverage, hence computation takes approximately 25 minutes. In S2, S3, S4 and S5, B Grid has been lowered to 21 arc-sec from 12 arc-sec. S4 and S5 also has a smaller coverage of the C Grid. S1, S2, and S5 shares the same A grid. The fastest computation time is S5, where the 10 hours of simulation time is completed in 9.06 minutes. For future forecasting capabilities the larger A Grid is preferred, which will be shared with all Puerto Rico grids, hence the S4 forecast model with a larger A Grid and still sufficient computation speed provides the

desired prediction and computation efficiency.

3.4 Model setup and validation

Table 2 summarizes the grid extents and model parameters of the reference and forecast models. The model parameters are similar to those used for other models in the SIFT system. A slightly higher Manning (friction) coefficient is used in the reference model to reduce high frequency, small-amplitude ringing that occurs along shorelines in the reference C grid with a lower coefficient.

Mayagüez forecast model is tested against two historical tsunamis. First scenario is a M_w 9.0 tsunami from Lisbon, Portugal adopted from Barkan et al. (2009) representing the 1755 tsunami. Source model for 1755 uses an elastic deformation (Smylie and Mansinha, 1971) with angles of Dip=40°,Strike=345°, and Rake=90° located at 10.7530°N, 36.0420°W and 5 km depth with a 26.5m slip on an area of 600×80 km. Second source is the 1918 Mona Passage tsunami with a unit source (1 m) rupture on ATSZ-52y matching the M_w 7.5 magnitude.

Forecast model predicts a 2m wave height from the 1755 Lisbon earthquake. This is a reasonable prediction amplitude for the region. 1918 is expected to be a submarine landslide (Lopez-Venegas et al., 2008) and the forecast model predicts a 75 cm wave height at the tide gauge, which is quite good considering that there is no landslide element and the published reports indicate that the maximum run up was approximately 1.1-15 m. Figure 7 for computed tide gauge prediction of the 1918 and 1755 tsunamis. Since the two scenarios tested for Mayagüez forecast model are quite good, model proves to be reliable for forecasting capabilities. More testing will be performed in the future as the tide records become available.

Chapter 4

Results

Validation of the forecast model ensures that, to the greatest extent possible, the model accurately reproduces actual tsunami events, and that it remains numerically stable under all possible source conditions (Synolakis et al., 2008; Tang et al., 2009).

Reference model and forecast models listed in Table 2 are tested against vigorous hypothetical scenarios. These scenarios ranges from Micro-tsunamis to Mega-tsunamis and are located in various locations of the Atlantic Ocean. Figure 8 shows the map of the Caribbean and South Atlantic Ocean with the location of synthetic scenarios used to test Mayagüez, Puerto Rico. For more details of the NOAA propagation database please see Gica et al. (2008) and Appendix B. Results of the all five forecast models and reference Model comparison with the test scenarios listed in Table 3 at the Mayaüez tide station are shown in Figure 9. All models agree each other fairly well for requirements of the tsunami prediction (Synolakis et al., 2008). Even though, any of the forecast models can be used for warning purposes, because of the system requirements, time optimization and model S4 has been designated in this study.

One of the interesting question arose during the development of the model was the height of the reflective boundaries in A and B grids. In Pacific Ocean models, depending on circumstances different reflective boundaries are applied for different model. In Caribbean models, because of the shallow reefs a development of not more than a meter reflective boundary is proposed by NOAA's Tsunami Research Center. S4 forecast model is test for sensitivity of response of 1 m and 10 m reflective boundaries in A and B grids at the Mayagüez tide station are shown in Figure 10. Proposed Mayagüez model has 1 m reflective boundary in A and B grids to be consistent with the other Caribbean models; however, according to this study accuracy between a model with 10 m and 1 m reflective boundary are negligible. In the future if need to be, the developer suggest that a 10 m reflective boundary can be used with confidence.

Forecast models are tested for 6 Synthetic tsunamis triggered from a hypothetical M_w 9.3 tsunamis with a 25 m rupture, 1 moderate tsunami from a M_w 7.5 earthquake with a 1 m rupture and a micro tsunami triggered from South Sandwich Islands from a 0.1 rupture for stability and reliability analysis. Test scenarios are listed in Table 3 and Figures 11, 12, 13, 14, 15, 17, 16, and 18 show the computed maximum amplitudes and maximum current speeds. Maximum and minimum amplitudes computed at the synthetic tide gauge are listed in Table 4 for comparison. Each scenario computed with the Reference Model and the forecast Model S4 as well as the rest of the models show good agreement with each other.

This study concludes that Muertos Trough in the South and Puerto Rico Trench in the North

are the potential tsunami threat for Mayagüez, Puerto Rico. Forecast model predicts an 8 m wave triggered from a M_w 9.3 earthquake from Puerto Rico Trench (ATSZ-48) and a 5 m wave from Muertos Trough (ATSZ-82) computed at the Mayagüez tide station listed in Table 4 and the corresponding maximum amplitude plots shown in Figures 12 and 15.

Chapter 5

Summary and Conclusions

This report describes the development of a real-time tsunami forecast model for Mayagüez, Puerto Rico. The forecast model grids were designed by comparing the results from multiple candidate grids to a reference model, for a variety of source scenarios. This algorithm for developing an optimal grid configuration may, with further refinement, be possible to automate, speeding inundation forecast model development.

The resulting forecast model is capable of producing real-time prediction of wave amplitudes and inundation that compare well with a higher-resolution reference model used for validation. Please note that both the reference and forecast model adequately predicts the synthetic events fairly well and the forecast model used in this report is good enough for the forecasting capabilities. Development of this optimized tsunami forecast model was based on a digital elevation model provided by the National Geophysical Data Center and the author considers it to be an adequate representation of the local topography/bathymetry. As new digital elevation models become available, forecast models will be updated and report updates will be posted at
http://nctr.pmel.noaa.gov/forecast_reports/.

Chapter 6

Acknowledgments

Special thank you to Marie Eble from Pacific Marine and Environmental Laboratories (National Oceanic and Atmospheric Adminisstration) and Lindsey Wright from Joint Institute of the Study of Ocean and Atmosphere (University of Washington) who had provided helpful assistance in locating the Mayagüez tide station and valuable information with the tide records. Lindsey Wright has also helped completing the SIFT testing of the forecast model. Mayagüez forecast model has been initially developed and designed by Aurelio Mercado and Wilford Schmidt from Department of Marine Sciences, University of Puerto Rico.

This work is funded by the Joint Institute for the Study of the Atmosphere and Ocean (JISAO) under NOAA Cooperative Agreement Numbers NA10OAR4320148 and NA08OAR4320899 and is JISAO contribution number No. 2152. This work is also Contribution No. XXXX from NOAA/Pacific Marine Environmental Laboratory.

Chapter 7

References

Baptista, M., Heitor, S., Miranda, J., Miranda, P., and Victor, L. (1998). The 1755 lisbon tsunami; evaluation of the tsunami parameters. *Journal of Geodynamics*, 25(1âĂŞ2):143 – 157.

Baptista, M. A., Miranda, J. M., Chierici, F., and Zitellini, N. (2003). New study of the 1755 earthquake source based on multi-channel seismic survey data and tsunami modeling. *Natural Hazards and Earth System Science*, 3(5):333–340.

Barkan, R. and ten Brink, U. (2010). Tsunami simulations of the 1867 virgin island earthquake: Constraints on epicenter location and fault parameters. *Bulletin of the Seismological Society of America*, 100(3):995–1009.

Barkan, R., ten Brink, U. S., and Lin, J. (2009). Far field tsunami simulations of the 1755 lisbon earthquake: Implications for tsunami hazard to the u.s. east coast and the caribbean. *Marine Geology*, 264(1âĂŞ2):109 – 122. <ce:title>Tsunami hazard along the U.S. Atlantic coast</ce:title>.

Eble, M. C. and González, F. I. (1991/04/01). Deep-ocean bottom pressure measurements in the northeast pacific. *Journal of Atmospheric and Oceanic Technology*, 8(2):221–233.

Gica, E., Spillane, M., Titov, V., Chamberlin, C., and Newman, J. (2008). Development of the forecast propagation database for NOAA's Short–term Inundation Forecast for Tsunamis (SIFT). Tech. Memo. OAR PMEL–139, NOAA/Pacific Marine Environmental Laboratory, Seattle, WA.

Granja Bruña, J. L., Ten Brink, U. S., Carbó Gorosabel, A., Muñoz Martín, A., and Gómez Ballesteros, M. (2009). Morphotectonics of the central muertos thrust belt and muertos trough (northeastern caribbean). *Marine Geology*, 263:7–33.

Harbitz, C., Glimsdal, S., Bazin, S., Zamora, N., Løvholt, F., Bungum, H., Smebye, H., Gauer, P., and Kjekstad, O. (2012). Tsunami hazard in the caribbean: Regional exposure derived from credible worst case scenarios. *Continental Shelf Research*, 38:1–23.

History.com (2013). U.S. takes control of Puerto Rico. http://www.history.com/this-day-in-history/us-takes-control-of-puerto-rico.

Lander, J. and Whiteside, L. (2007). Caribbean Tsunamis: An Initial History. In *Tsunami Workshop June 11Ð13*, Mayaguez, Puerto Rico.

Lopez-Venegas, A. M., ten Brink, U. S., and Geist, E. L. (2008). Submarine landslide as the source for the october 11, 1918 mona passage tsunami: Observations and modeling. *Marine Geology*, 254(1):35–46.

National Geophysical Data (2013). (NGDC) Historic Tsunami Data Base. http://www.ngdc.noaa.gov/seg/hazard/tsu.shtml.

O'Loughlin, K. and Lander, J. (2003). *Caribbean Tsunamis, A 500-Year History from 1498Ð1998*. Springer, The Netherlands, second edition edition.

Smithsonian Magazine (2013). Puerto Rico – History and Heritage. http://www.smithsonianmag.com/travel/destination-hunter/north-america/caribbean-atlantic/puerto-rico/puerto-rico-history-heritage.html.

Smylie, D. E. and Mansinha, L. (1971). The elasticity theory of dislocations in real earth models and changes in the rotation of the earth. *Geophys. J. R. astr. Soc.*, 23:329–354.

Synolakis, C. E., Bernard, E., Titov, V., Kânoğlu, U., and González, F. (2008). Validation and verification of tsunami numerical models. *Pure Appl. Geophys*, 165:2197–2228.

Tang, L., Chamberlin, C., and Titov, V. (2008a). Developing tsunami forecast inundation models for Hawaii: procedures and testing. Tech. Memo. OAR PMEL-141, NOAA.

Tang, L., Chamberlin, C., Tolkova, E., Spillane, M., Titov, V., Bernard, E., and Mofjeld, H. (2006). Assessment of potential tsunami impact for Pearl Harbor, Hawaii. Tech. Memo. OAR PMEL, NOAA.

Tang, L., Titov, V., and Chamberlin, C. (2009). Development, testing, and applications of site-specific tsunami inundation models for real-time forecasting. *J. Geophys. Res*, page C12025.

Tang, L., Titov, V., Wei, Y., Mofjeld, H., Spillane, M., Arcas, D., Bernard, E., Chamberlin, C., Gica, E., and Newman, J. (2008b). Tsunami forecast analysis for the may 2006 tonga tsunami. *J. Geophys. Res*, page C12015.

Taylor, L., Eakins, B., Carignan, K., Warnken, R., Sazonova, T., and Schoolcraft, D. (2007). Digital Elevation Models for Puerto Rico: Procedures, Data Sources and Analysis. NOAA Technical Memorandum, NOAA, National Geophysical Data Center, Marine Geology and Geophysics Division, Boulder, Colorado.

Titov, V. V. (2009). *Tsunami forcasting*, volume 15: Tsunamis of *the Sea*, chapter 12, pages 371–400. Harvard University Press, Cambridge, MA and London, England.

Titov, V. V. and González, F. (1997). Implementation and testing of the method of splitting tsunami (MOST) model. Technical Memorandum ERL PMEL 112, NOAA.

Titov, V. V., González, F. I., Bernard, E. N., Eble, M. C., Mofjeld, H. O., Newman, J. C., and Venturato, A. J. (2005). Real-Time Tsunami Forecasting: Challenges and Solutions. *Natural Hazards*, 35(1):35–41.

Titov, V. V. and Synolakis, C. E. (1998). Numerical modelling of tidal wave runup. *J. Waterw. Port Coast. Ocean Eng.*, 124:157–171.

U.S. Census Bureau (2012). Metropolitan and Micropolitan Statistical Areas Totals: Vintage 2012. http://http://www.census.gov/popest/data/metro/totals/2012/index.html.

Uslu, B., Eble, M., Arcas, D., and Titov, V. (2013). Tsunami Hazard Assessment for the Commonwealth of the Northern Mariana Islands. Tsunami Hazard Assessment Special Series, NOAA.

Uslu, B., Eble, M., and Chamberlin, C. (2010a). Tsunami Hazard Assessment for Guam. Tsunami Hazard Assessment Special Series, NOAA OAR Special Repor.

Uslu, B., Eble, M., Titov, V., and Bernard, E. (2010b). Distant tsunami threats to the ports of Los Angeles and Long Beach, California. Tsunami Hazard Assessment Special Series, NOAA OAR Special Report.

Vélez-Rodríguez, L. L. (2007a). Tidal Stations and Bench Marks: Tools for Spatial Information Managements. In *6th FIG Regional Conference* , TS 09 Ð Natural Resources and Risk Management, pages 1/9–9/9 pp., San José, Costa Rica.

Vélez-Rodríguez, L. L. (2007b). Tidal Stations and Bench Marks: Tools for Spatial Information Managements. *6th FIG Regional Conference* .

Wei, Y., Bernard, E. N., Tang, L., Weiss, R., Titov, V. V., Moore, C., Spillane, M., Hopkins, M., and glu, U. K. (2008). Real-time experimental forecast of the Peruvian tsunami of August 2007 for U.S. coastlines. *Geophys. Res. Let.*, 35:L04609.

Zahibo, N., Pelinovsky, E., Kurkin, A., and Nikolkina, I. (2008). Tunami hazard for the french west indies lesser antilles. In Krishnamurthy, R., Kannen, A., Ramanathan, A., Tinti, S., Glavovic, B. C., Green, D. R., Han, Z., and Agardy, T. S., editors, *Integrated Coastal Zone Management (ICZM)*, page 800 pp. Research Publishing Services, ISBN:978-981-05-8948-6.

Zahibo, N., Pelinovsky, E., Yalciner, A. C., Kurkin, A., Koselkov, A., and Zaitsev, A. (2003). The 1867 virgin island tsunami. *Natural Hazards and Earth System Science*, 3(5):367–376.

Zahibo, N. and Pelinovsky, E. N. (2001). Evaluation of tsunami risk in the lesser antilles. *Natural Hazards and Earth System Science*, 1(4):221–231.

FIGRUES

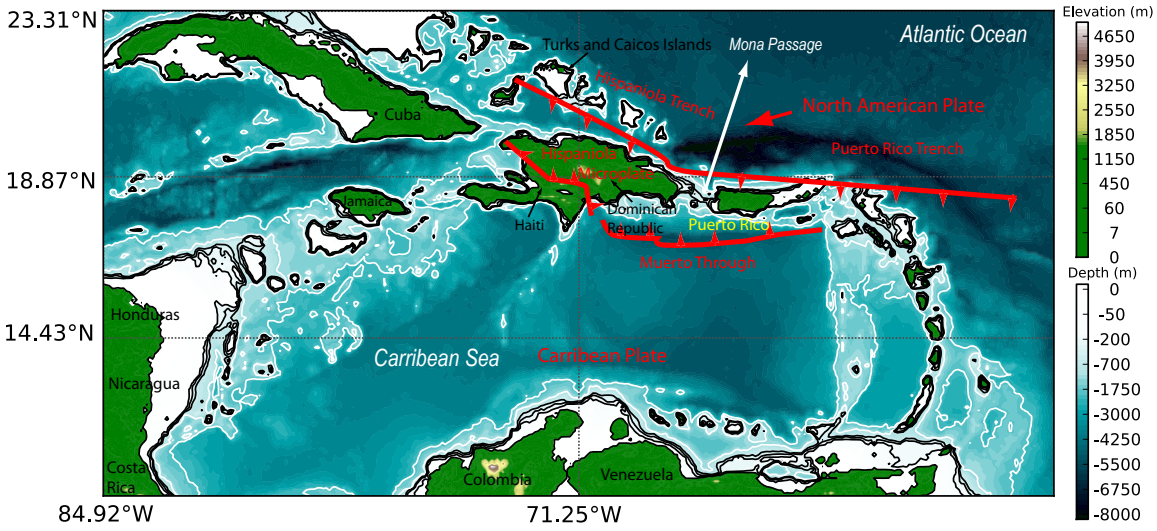

Figure 1: Location of Puerto Rico relative to the Caribbean Sea is shown. Plate motions are reproduce from Granja Bruña et al. (2009).

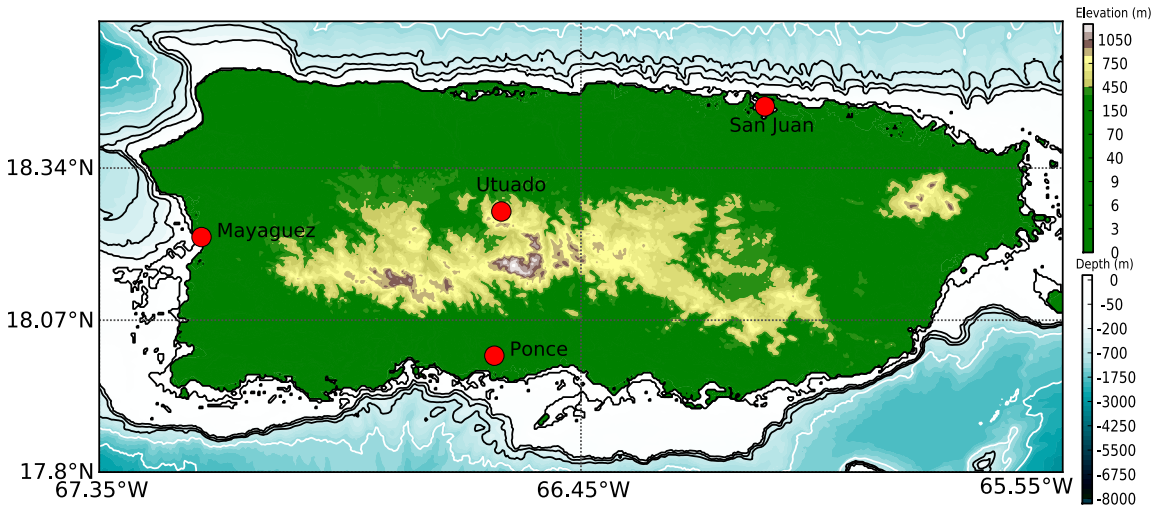

Figure 2: A digital elevation map of Puerto Rico that shows the location of Mayagüez with respect to the capital San Juan and Ponce.

Figure 3: Three images above show the location of Mayagẗez tide gauge. The large satellite overlay is s Google Earth image with the location of the tide gauge from Puerto Rico Seismic Network and Vélez-Rodríguez (2007a). Image of the NOAA tide station in the lower left corner is provided by Vélez-Rodríguez (2007a,b). Inset illustrating the the location of the tide station on a satellite image in the lower right corner is provided by Vélez-Rodríguez (2007b)

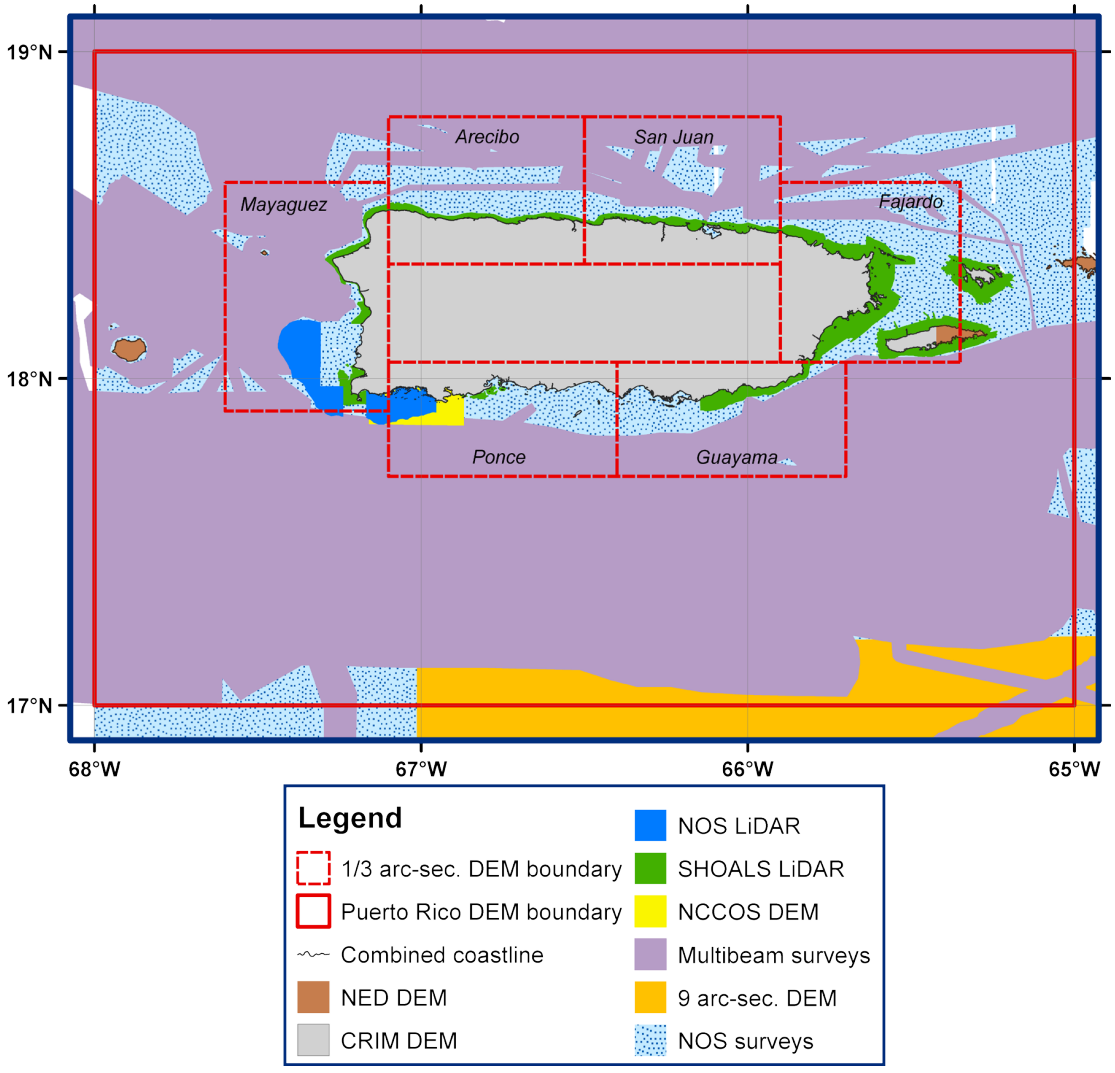

Figure 4: Sources used in the development of digital elevation map of Puerto Rico by NGDC are shown in the figure (Taylor et al., 2007).

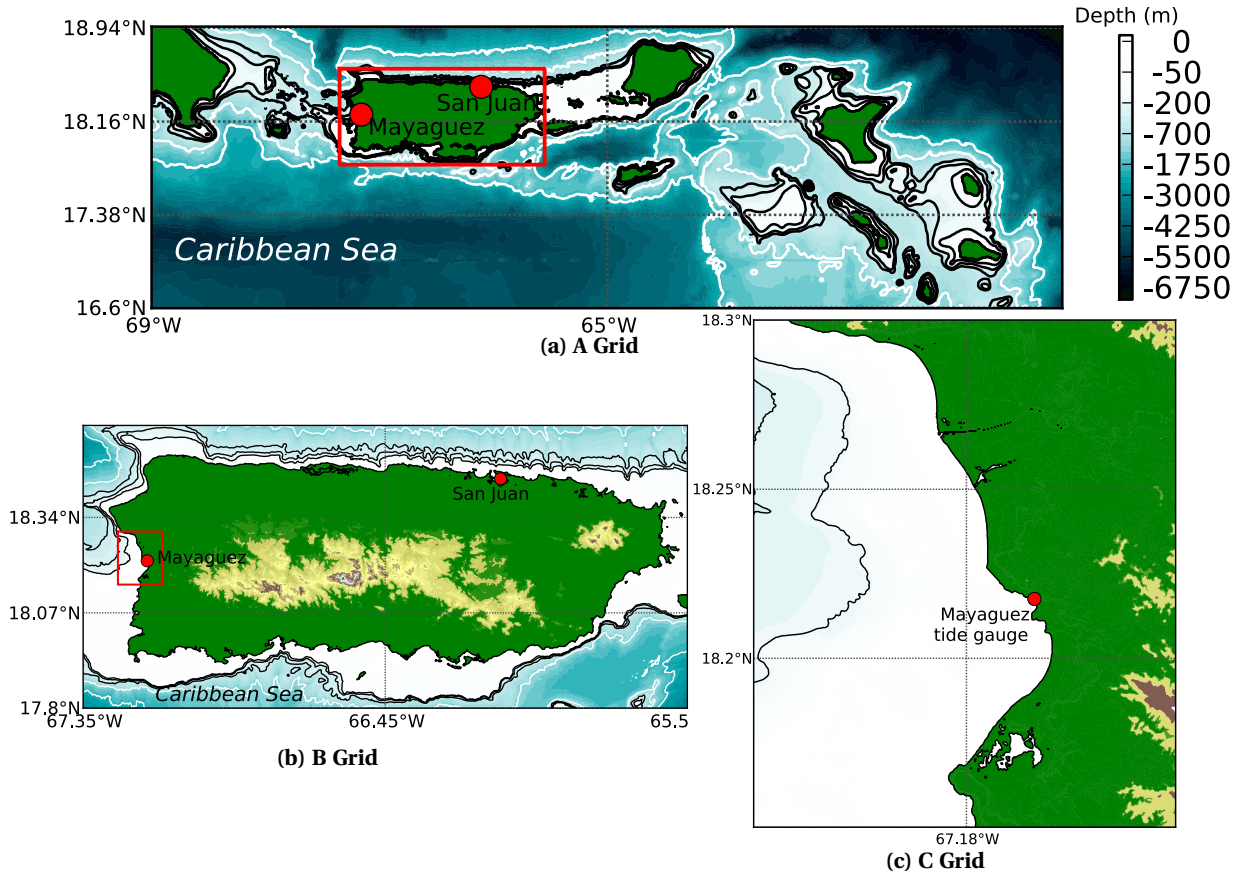

Figure 5: Reference model grids used for Mayagüez, Puerto Rico are shown above. (a) A grid, (b) B grid and (c) C grids are shown respectively. B grid covers the Puerto Rico as an island and location of the tide station is shown in the C grid.

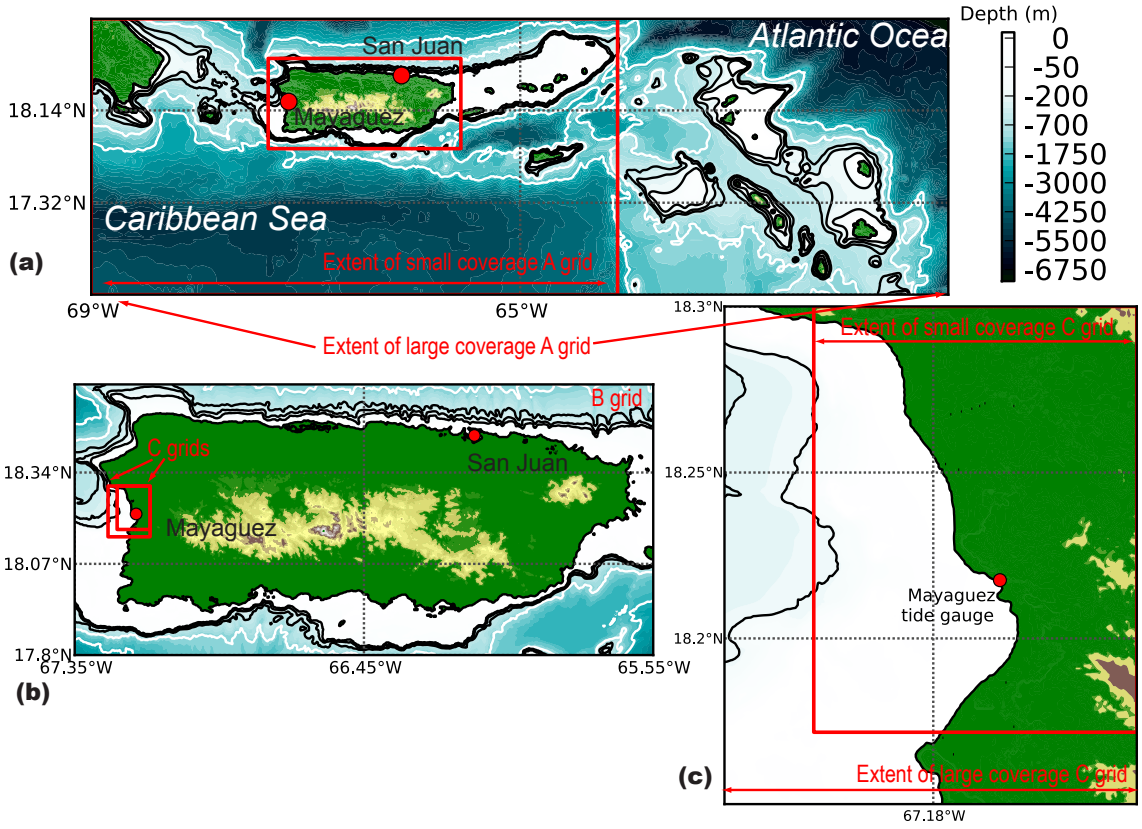

Figure 6: Six different grids are developed for five sets of forecast model. (a) Two A grids are designed with two different meridional extents. (b) Both B grids cover the same extends, but with different resolution. (c) Two different C grid extents are designed for optimal computation time. Location of the tide station is marked with red marker at Mayagüez.

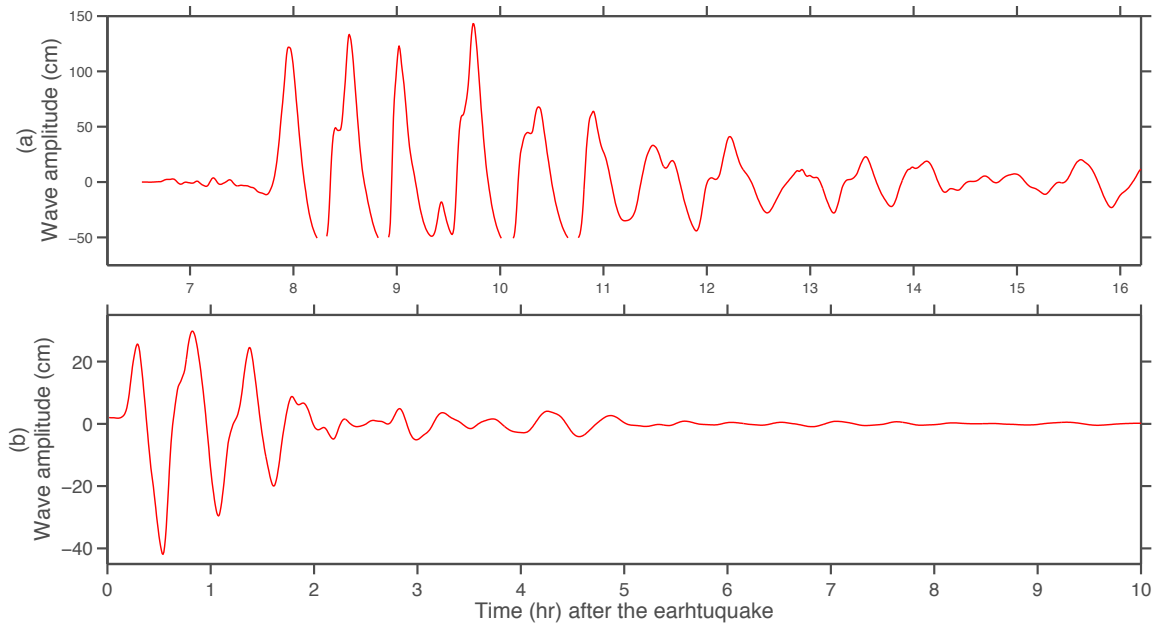

Figure 7: Computed tide gauge signals from (a) 1755 Lisbon Earthquake and (b) 1918 Mona Passage earthquakes are shown above.

Figure 8: Map of the Caribbean and South Atlantic Ocean showing the location of synthetic scenarios from Table 3 used to test Mayagüez, Puerto Rico Model are shown with the NOAA's propagation database.

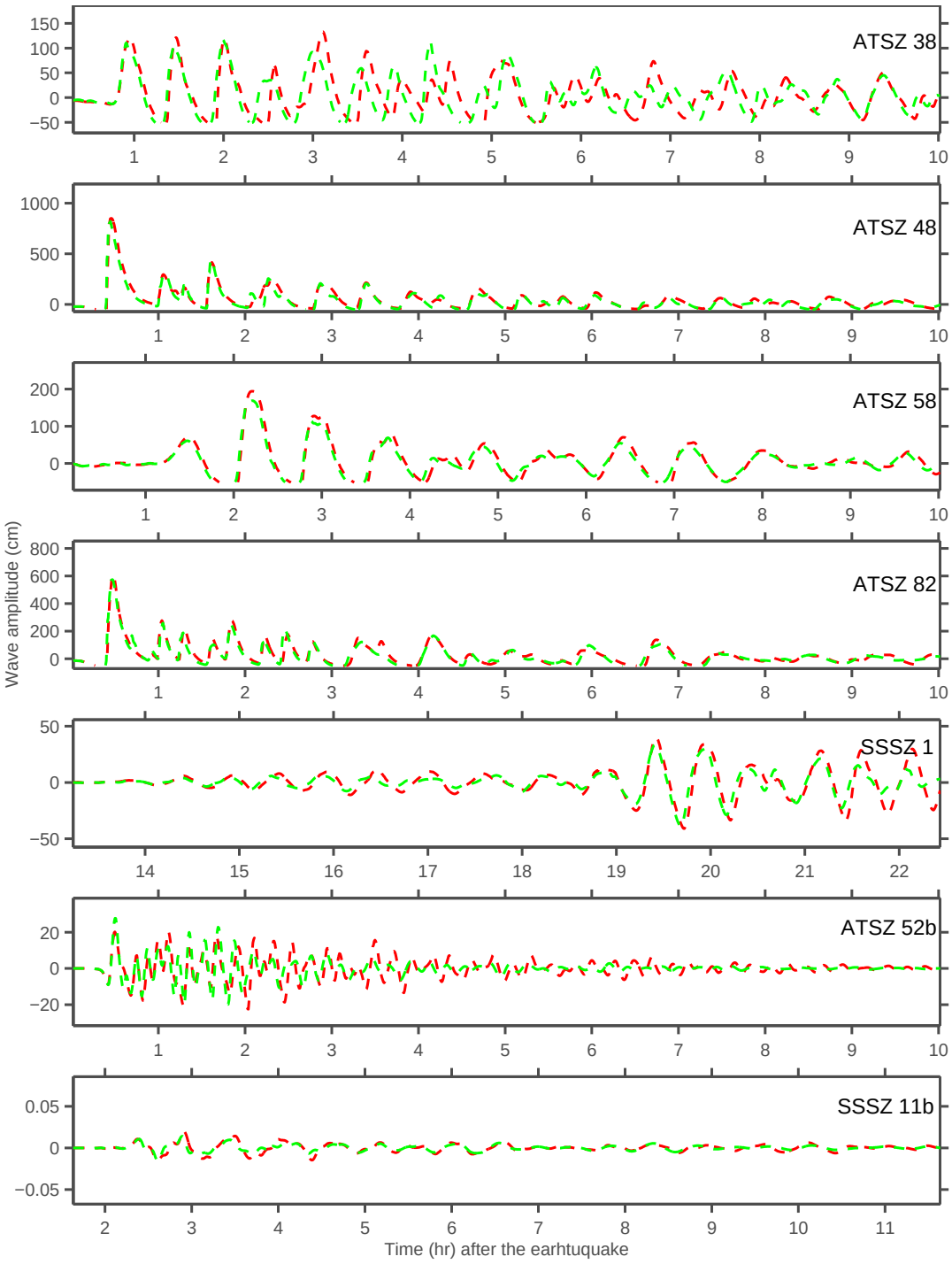

Figure 9: Reference model and Forecast models listed in Table 1 are tested against the hypothetical scenarios listed in Table 3. All five Forecast model and Reference Model agree fairly well for requirements for tsunami prediction (Synolakis et al., 2008).

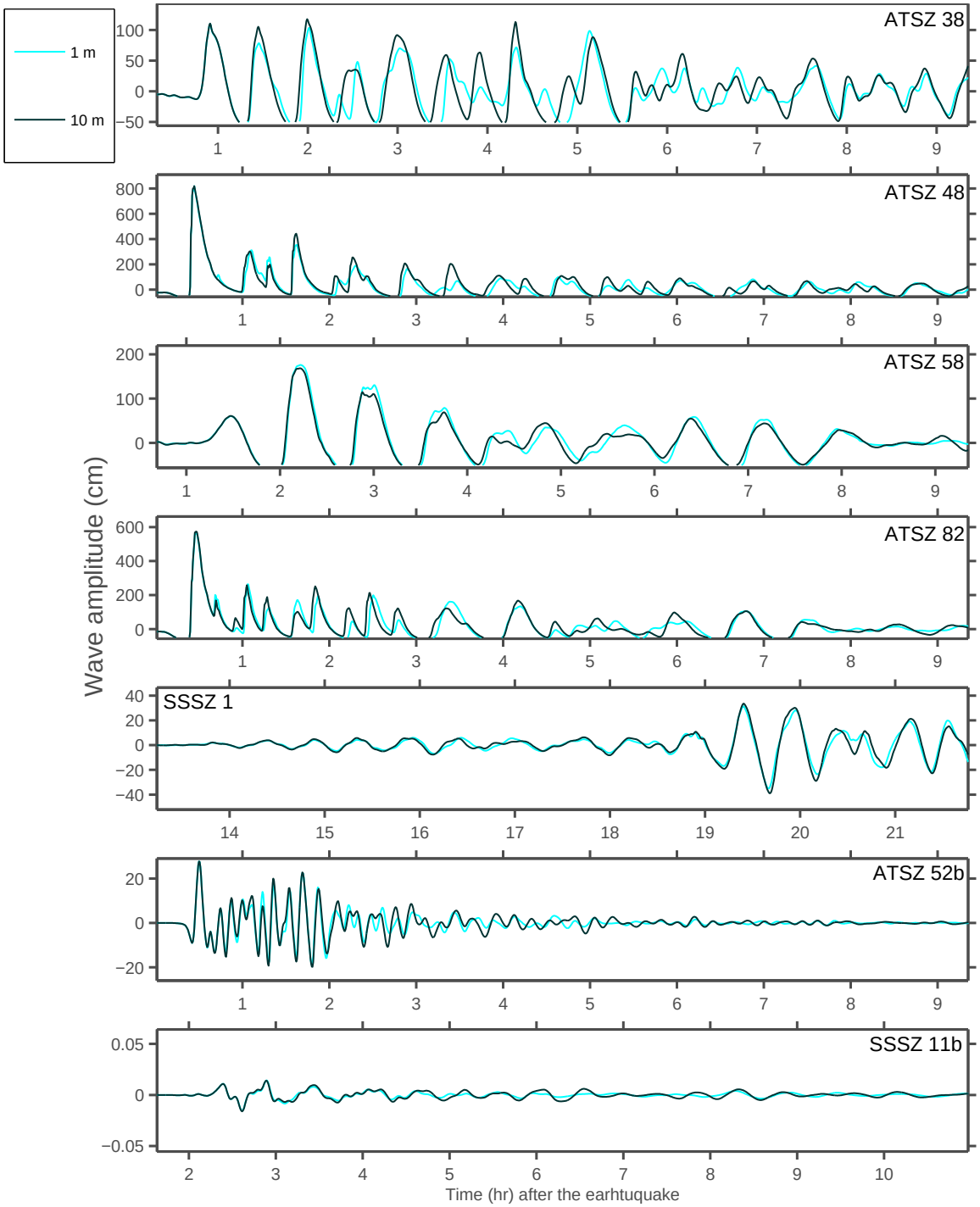

Figure 10: S4 Forecast model from the list in Table 3 is designated as the forecast model to be used by the warning centers. This forecast model is test for sensitivity of reflective boundary and the response of 1 m and 10 m reflective boundary at the Mayagüez tide station are shown above.

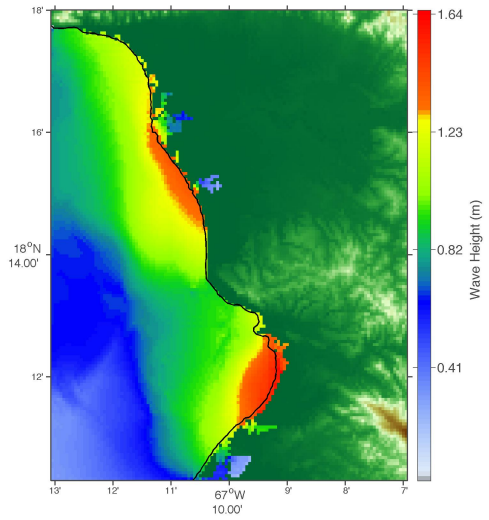

(a) Maximum amplitude for forecast model

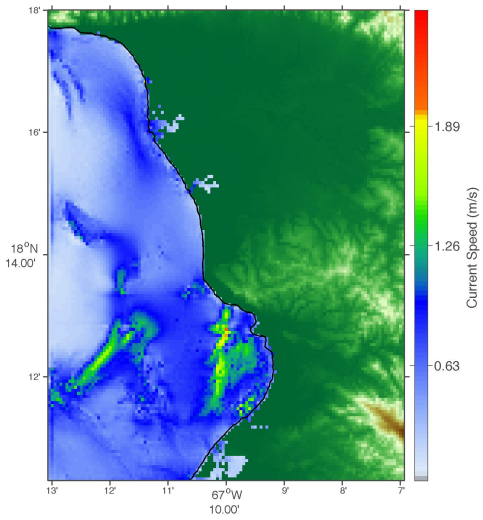

(b) Maximum current speed for forecast model

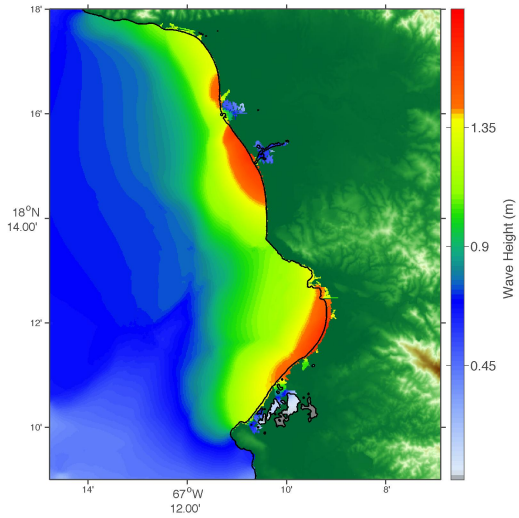

(c) Maximum amplitude for reference model

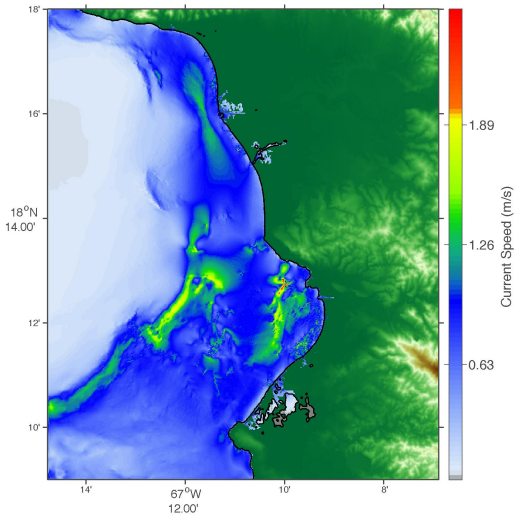

(d) Maximum current speed for reference model

Figure 11: Computed results of maximum amplitude and currents speed for a synthetic M_w 9.3 earthquake from ATSZ 38-47 are shown above for forecast and reference models.

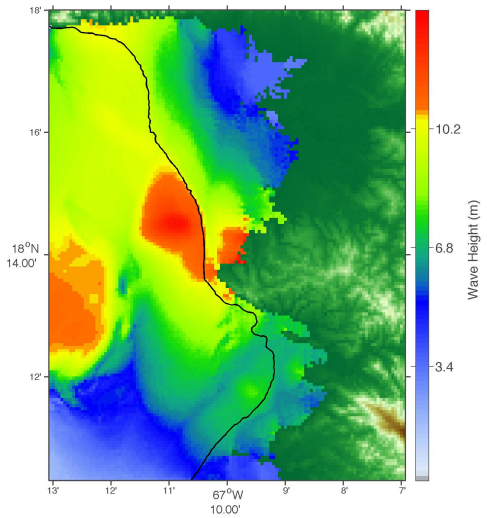

(a) Maximum amplitude for forecast model

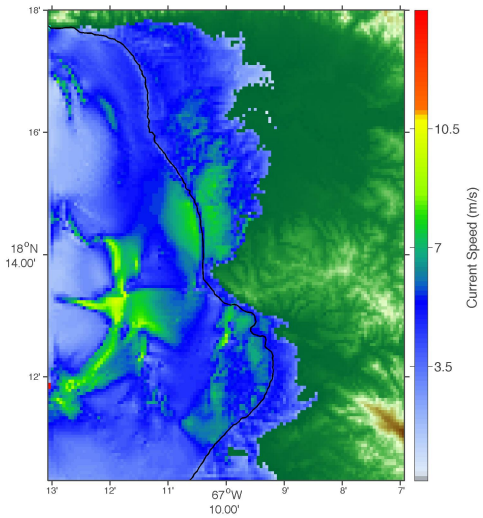

(b) Maximum current speed for forecast model

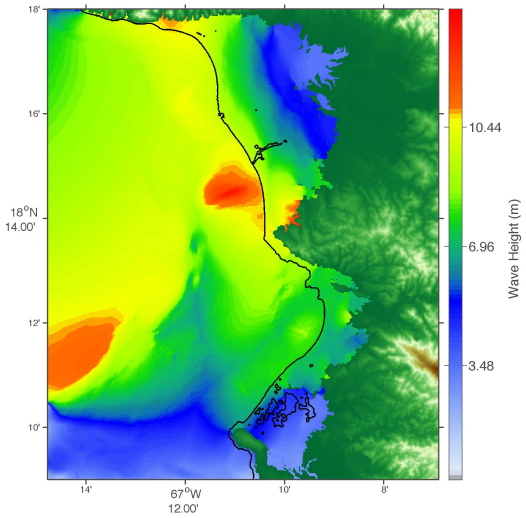

(c) Maximum amplitude for reference model

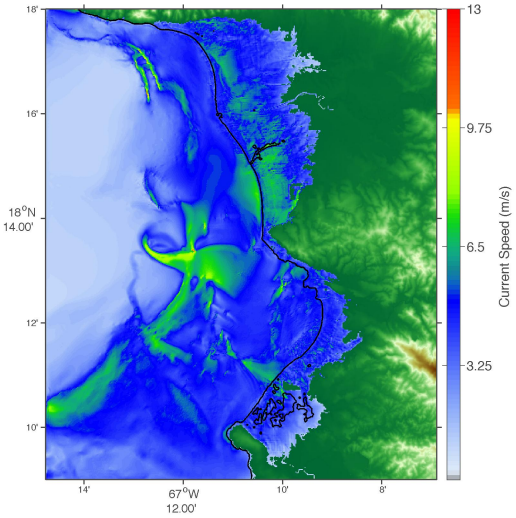

(d) Maximum current speed for reference model

Figure 12: Computed results of maximum amplitude and currents speed for a synthetic M_w 9.3 earthquake from ATSZ 48-57 are shown above for forecast and reference models.

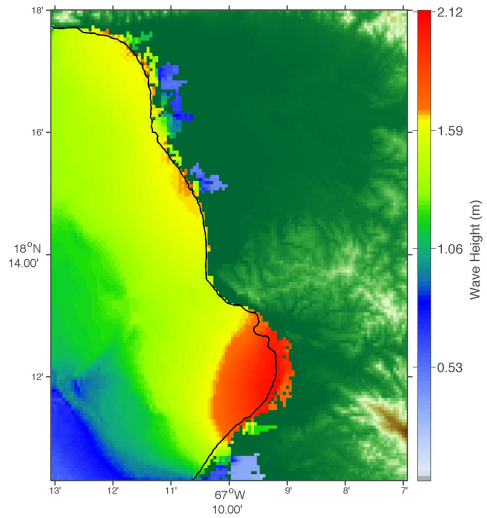

(a) Maximum amplitude for forecast model

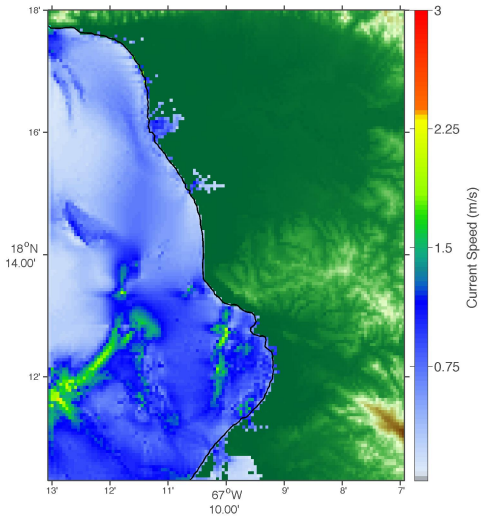

(b) Maximum current speed for forecast model

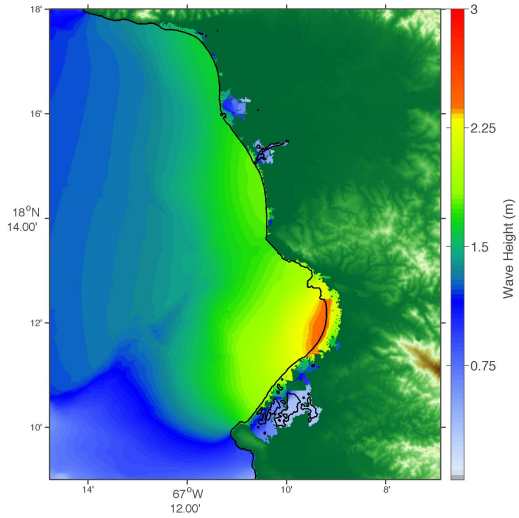

(c) Maximum amplitude for reference model

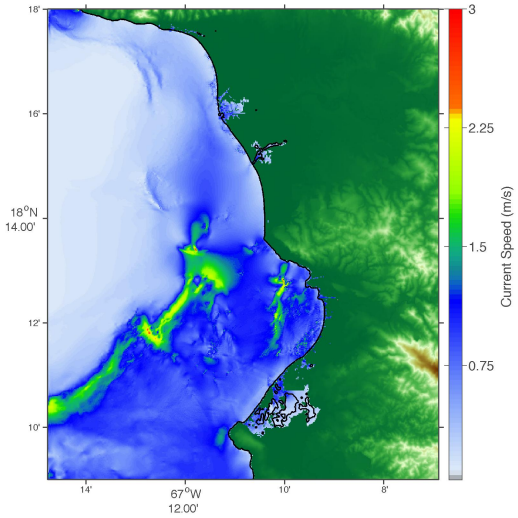

(d) Maximum current speed for reference model

Figure 13: Computed results of maximum amplitude and currents speed for a synthetic M_w 9.3 earthquake from ATSZ 58-67 are shown above for forecast and reference models.

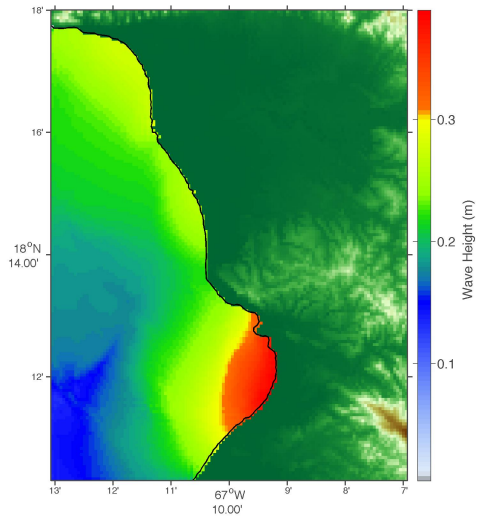

(a) Maximum amplitude for forecast model

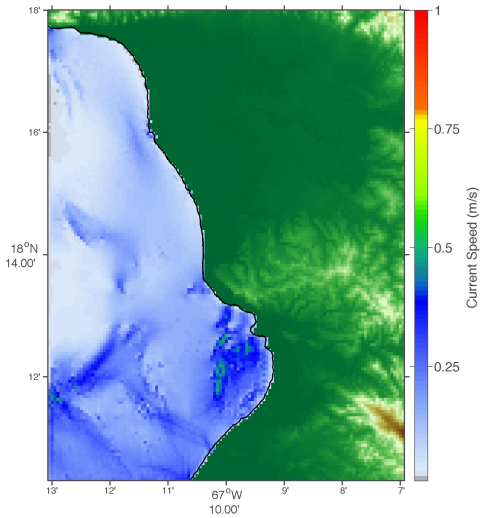

(b) Maximum current speed for forecast model

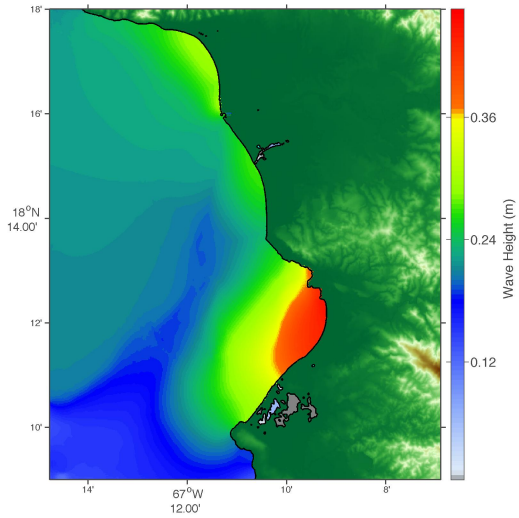

(c) Maximum amplitude for reference model

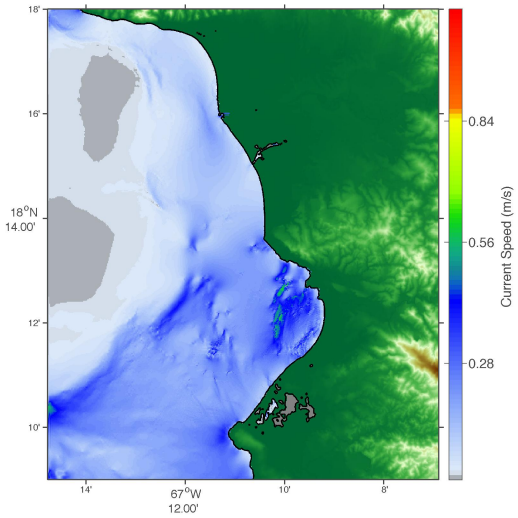

(d) Maximum current speed for reference model

Figure 14: Computed results of maximum amplitude and currents speed for a synthetic M_w 9.3 earthquake from ATSZ 68-77 are shown above for forecast and reference models.

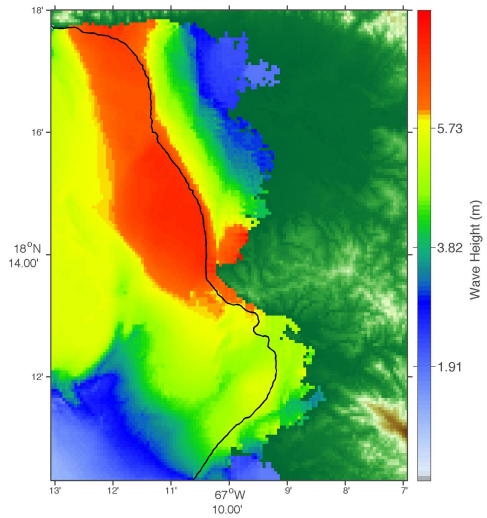

(a) Maximum amplitude for forecast model

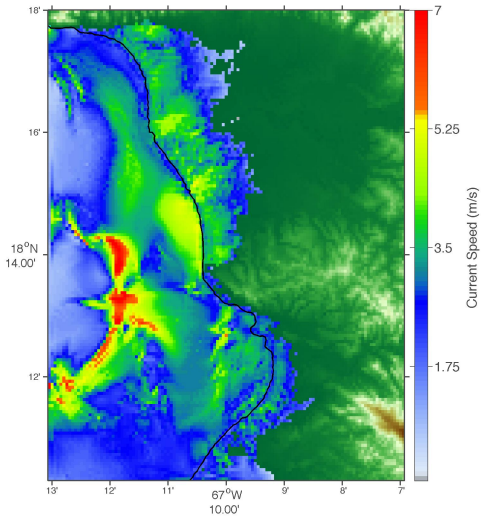

(b) Maximum current speed for forecast model

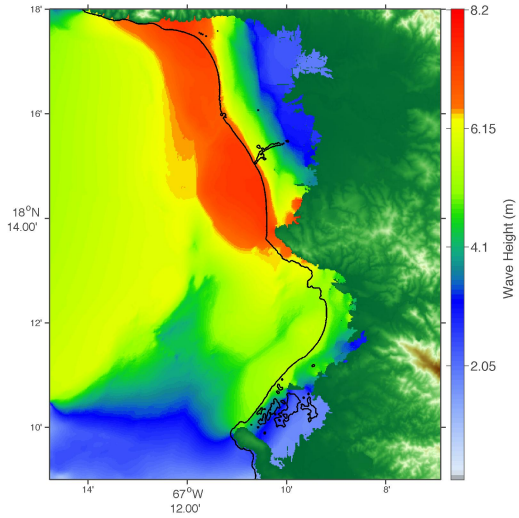

(c) Maximum amplitude for reference model

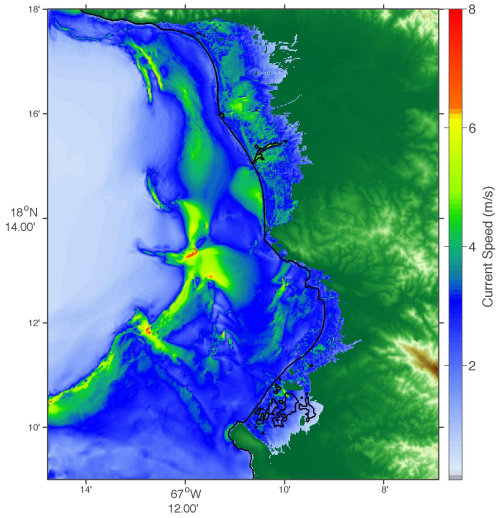

(d) Maximum current speed for reference model

Figure 15: Computed results of maximum amplitude and currents speed for a synthetic M_w 9.3 earthquake from ATSZ 82-91 are shown above for forecast and reference models.

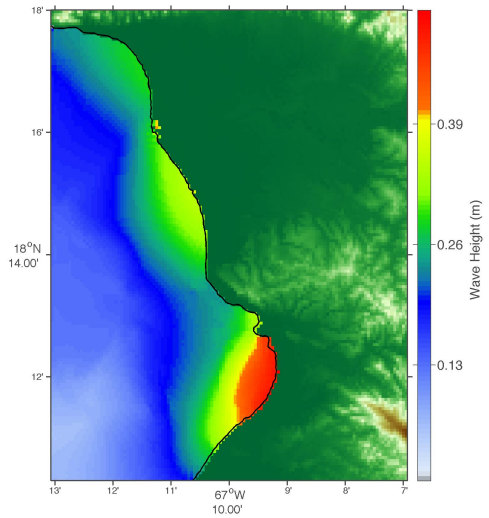

(a) Maximum amplitude for forecast model

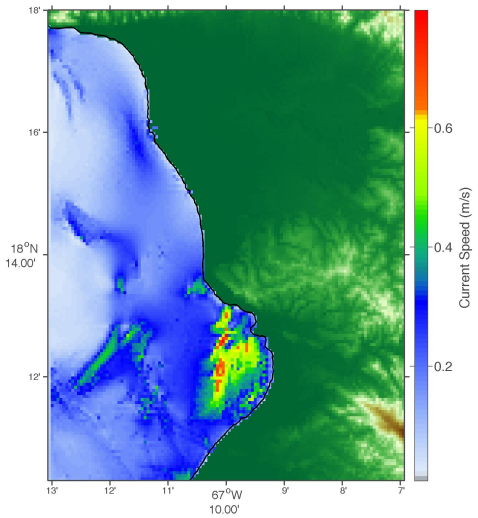

(b) Maximum current speed for forecast model

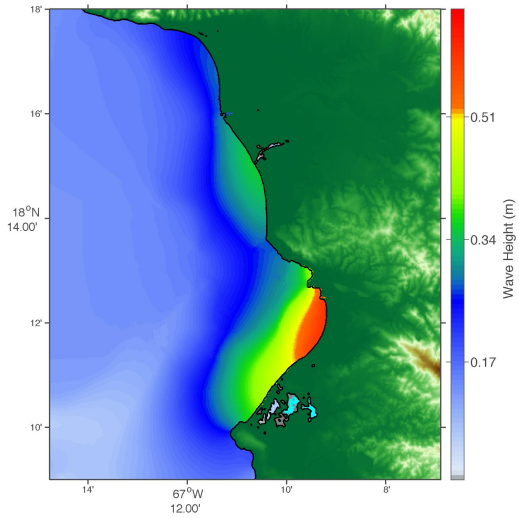

(c) Maximum amplitude for reference model

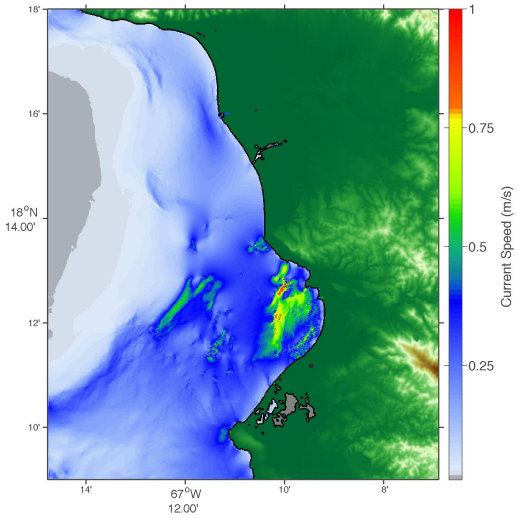

(d) Maximum current speed for reference model

Figure 16: Computed results of maximum amplitude and currents speed for a synthetic M_w 9.3 earthquake from SSSZ 1 are shown above for forecast and reference models.

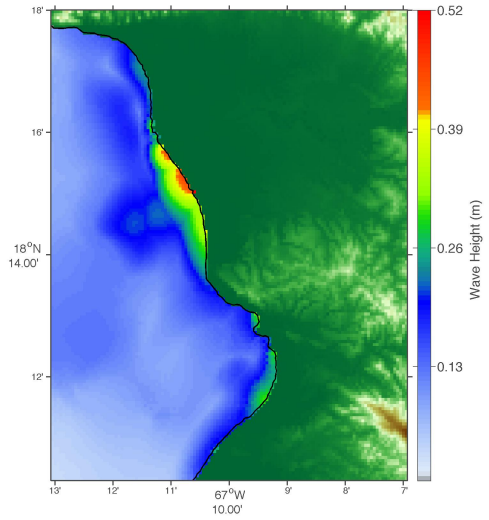

(a) Maximum amplitude for forecast model

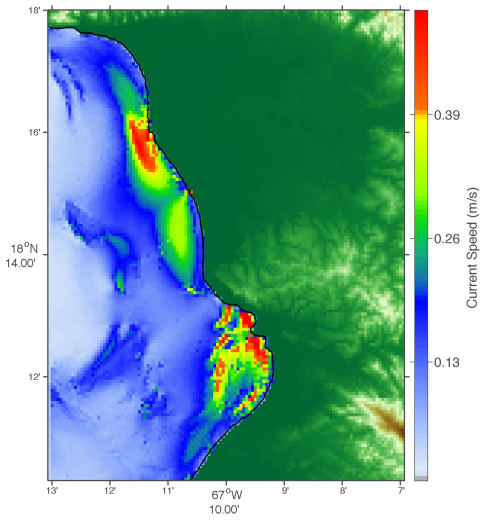

(b) Maximum current speed for forecast model

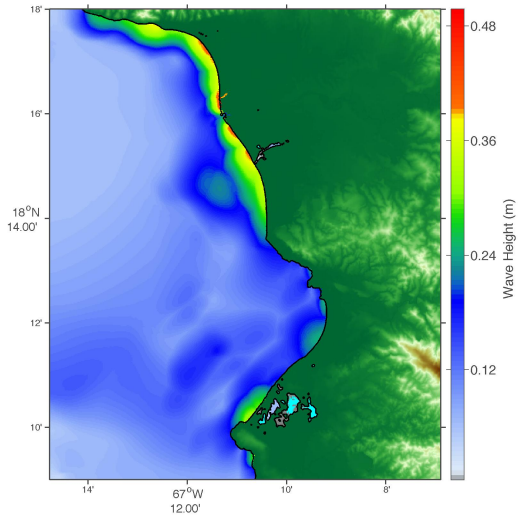

(c) Maximum amplitude for reference model

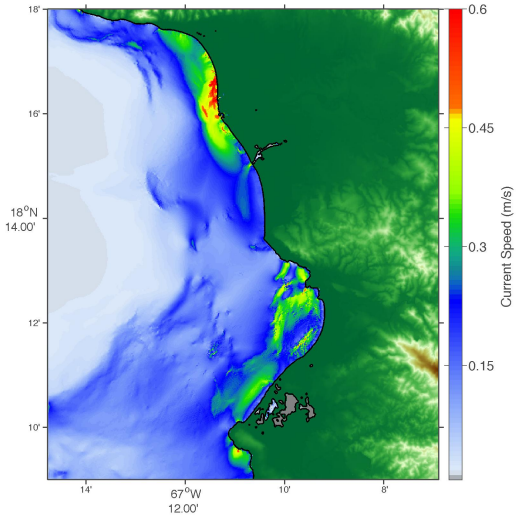

(d) Maximum current speed for reference model

Figure 17: Computed results of maximum amplitude and currents speed for a synthetic M_w 7.5 earthquake from ATSZ 52b are shown above for forecast and reference models.

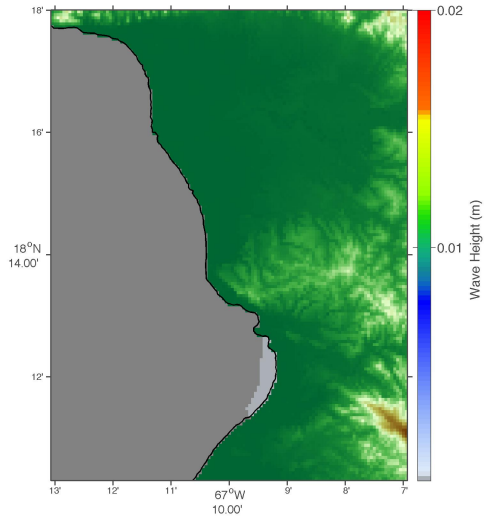

(a) Maximum amplitude for forecast model

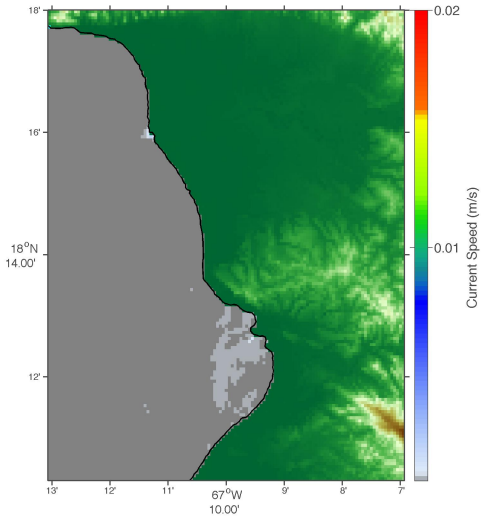

(b) Maximum current speed for forecast model

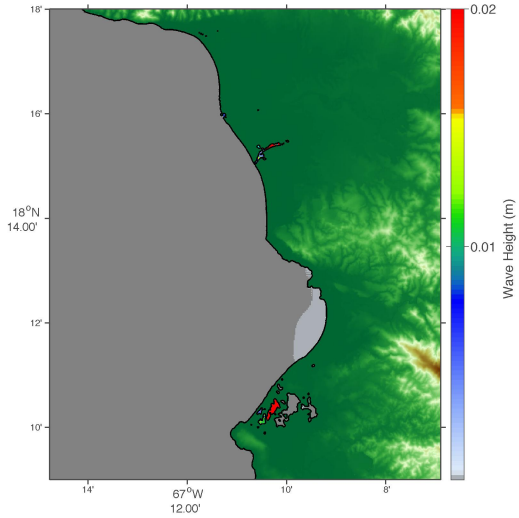

(c) Maximum amplitude for reference model

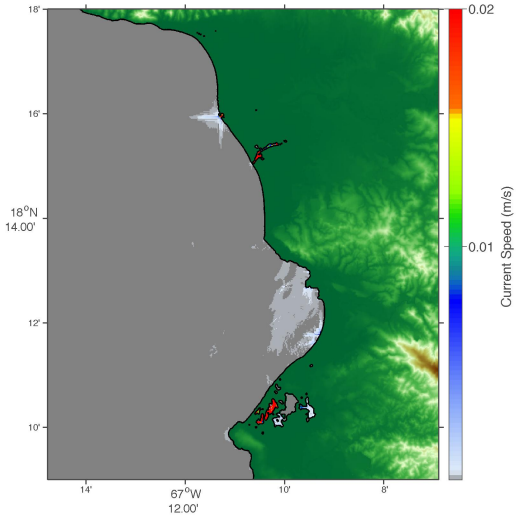

(d) Maximum current speed for reference model

Figure 18: Computed results of maximum amplitude and currents speed for a synthetic M_w 6.2 earthquake from SSSZ 11 with 0.1 m slip are shown above for forecast and reference models.

TABLES

Table 1: One reference model and a set of five forecast models are designed in this study. Designed five forecast model use difference variance of grids for optimal prediction and computation time.

Model Name	A Grid	B Grid	C Grid	Computation Time (min)
Reference model (R)	mayaguez_24s-ssl.1nod 24 arc-sec	mayaguez_6s_s2-ssl_1nod_c2-ssl 6 arc-sec	mayaguez_1s_s2_c-ssl.1nod 1 arc-sec	
Forecase model (S1)	A5_45s_1nd_SSL1.9.asc.topo1 45 arc-sec Larger coverage	SJ_grid_B-ssl_1nod 12 arc-sec Higher resolution	mayaguez_3s_s_1n_c-ssl 3 arc-sec Larger coverage	25.0167
Forecase model (S2)	A5_45s_1nd_SSL1.9.asc.topo1 45 arc-sec Larger coverage	mayaguez_21s-ssl 21 arc-sec Lower resolution	mayaguez_3s_s_1n_c-ssl 3 arc-sec Larger coverage	16.6000
Forecase model (S3)	mayaguez_45s-ssl.1nod 45 arc-sec Smaller coverage	mayaguez_21s-ssl 21 arc-sec Lower resolution	mayaguez_3s_s_1n_c-ssl 3 arc-sec Larger coverage	12.0167
Forecase model (S4)	A5_45s_1nd_SSL1.9.asc.topo1 45 arc-sec Larger coverage	mayaguez_21s-ssl 21 arc-sec Lower resolution	mayaguez_3s_s2-ssl 3 arc-sec Smaller coverage	12.767
Forecase model (S5)	mayaguez_45s-ssl.1nod 45 arc-sec Smaller coverage	mayaguez_21s-ssl 21 arc-sec Lower resolution	mayaguez_3s_s2-ssl 3 arc-sec Smaller coverage	9.0667

Table 2: MOST setup parameters for reference and forecast models for Mayagüez, Puerto Rico.

		Reference Model				Forecast Model			
Grid	Region	Coverage Lat. [°N] Lon. [°W]	Cell Size ["]	nx x ny	Time Step	Coverage Lat. [°N] Lon. [°W]	Cell Size ["]	nx x ny	Time Step
A	North East Caribbean Sea	16.597–18.950 291.000–298.993	24	1200 × 354	2.25	16.500–18.950 18.950–18.950	47	610 × 197	4.00
B	Puerto Rico	17.800–18.600 292.650–294.450	6	1081 × 481	0.45	17.801–18.600 18.600–18.600	21	309 × 138	2.00
C	Mayagüez	18.150–18.300 292.754–292.885	1	474 × 541	0.45	18.172–18.300 18.300–18.300	3	124 × 155	2.00
Minimum offshore depth [m]:		10.0				1.0			
Water depth for dry land]m]:		0.1				0.1			
Friction coffeficient [n^2]:		0.004				0.003			
CPU time for 10-hr simulation:		392.2334 mins				12.7667 mins			

Computations were performed on a single Intel Xeon processor at 2.93GHz, PowerEdge R510.

Table 3: Synthetic tsunami events used in development of Mayagüez, Puerto Rico Forecast Model.

Scenario No	Scenario Name	Source Zone	Tsunami Source Parameters	α (m)
		Mega-tsunami Scenarios		
1	ATSZ 38	Atlantic	A38-A47, A38-A47	25
2	ATSZ 48	Atlantic	A48-A57, B48-B57	25
3	ATSZ 58	Atlantic	A58-A67, B58-B67	25
4	ATSZ 68	Atlantic	A68-A77, B68-B77	25
5	ATSZ 82	Atlantic	A82-A91, B82-B91	25
6	SSSZ 1-10	South Sandwich	A1-A10, B1-B10	25
		M_w 7.5-tsunami Scenario		
7	ATSZ B52	Atlantic	B52	1
		Micro-tsunami Scenario		
8	SSSZ B11	South Sandwich	B11	0.01

Table 4: Maximum and minimum amplitude computed during the development of Mayagüez, Puerto Rico forecast Models are listed below.

		Reference Model		S1		S2		S3		S4		S5	
Scenario	M_w	Max. Amp. (cm)	Min. Amp (cm)	Max. Amp. (cm)	Min. Amp. (cm)	Max. Amp. (cm)	Min. Amp. (cm)	Max. Amp. (cm)	Min. Amp. (cm)	Max. Amp. (cm)	Min. Amp. (cm)	Max. Amp. (cm)	Min. Amp. (cm)
ATSZ-38	9.3	132.95	-50.76	133.87	-50.91	127.48	-50.93	136.24	-51	110.1	-51	117.71	-50.97
ATSZ-48	9.3	849.8	-50.65	863.8	-50.95	867	-51	866.34	-50.91	818.95	-50.93	819.71	-50.94
ATSZ-58	9.3	193.83	-50.85	209.54	-51	208.36	-50.94	208.39	-50.99	176.19	-50.76	168.59	-50.94
ATSZ-68	9.3	36.9	-36.09	40.98	-39.5	39.89	-38.64	39.83	-38.57	31.07	-28.21	31.71	-29.28
ATSZ-82	9.3	609.95	-51	630.88	-50.85	626.08	-50.88	626.23	-50.8	564.27	-51	573.76	-50.75
SSSZ-1	9.3	39.92	-41.05	44.34	-47.35	42.98	-46.1	42.08	-45.9	31.41	-35.09	33.54	-38.91
ATSZ-B52	7.5	20.4	-22.52	23.51	-23.63	24.18	-22.39	24.16	-22.31	27.73	-19.03	27.72	-19.83
SSSZ B11	6.2	0.02	-0.01	0.02	-0.02	0.02	-0.02	0.02	-0.02	0.01	-0.02	0.01	-0.02

Appendix A

A.1 Forecast model ⋆.in file for Mayagüez, Puerto Rico:

0.00001 Minimum amp. of input offshore wave (m)
1.0 Minimum depth of offshore (m)
0.1 Dry land depth of inundation (m)
0.003 Friction coefficient (n⋆⋆2)
1 Let A-Grid and B-Grid run up
300.0 Max eta before blow-up (m)
2.0 Time step (sec)
18000 Total number of time steps in run (6 hours)
2 Time steps between A-Grid computations
1 Time steps between B-Grid computations
14 Time steps between output steps
0 Time steps before saving first output step
1 Save output every n-th grid point
mayaguez_run2d/A5_45s_1nd_SSL1.9.asc.topo1
mayaguez_run2d/mayaguez_21s-ssl_1n
mayaguez_run2d/mayaguez_3s_s2-ssl
./
./
1 1 1 1 NetCDF output for A, B, C, SIFT
1 Timeseries locations: 3 71 101 mayaguez nearest grid point to 292.8404167 E, 18.21671295 N

A.2 Reference model ⋆.in file for Mayagüez, Puerto Rico:

0.001 Minimum amp. of input offshore wave (m)
10 Minimum depth of offshore (m)
0.1 Dry land depth of inundation (m)
0.004 Friction coefficient (n⋆⋆2)
1 Let A-Grid and B-Grid run up
300.0 Max eta before blow-up (m)
0.45 Time step (s)
80000 Total number of time steps in run (4.0 hours)
5 Time steps between A-grid computations
1 Time steps between B-grid computations
70 Time steps between output steps
0 Time steps before saving first output step
2 Save output every n-th grid point
mayaguez_24s-ssl.1nod
mayaguez_6s_s2-ssl_1nod_c2-ssl
mayaguez_1s_s2_c-ssl.1nod
./
./
1 1 1 1 NetCDF output for A, B, C, SIFT
1 Timeseries locations:
3 313 301 mayaguez nearest grid point to 292.8404167 E, 18.21671295 N

Appendix B

Propagation Database: Atlantic Ocean Unit Sources

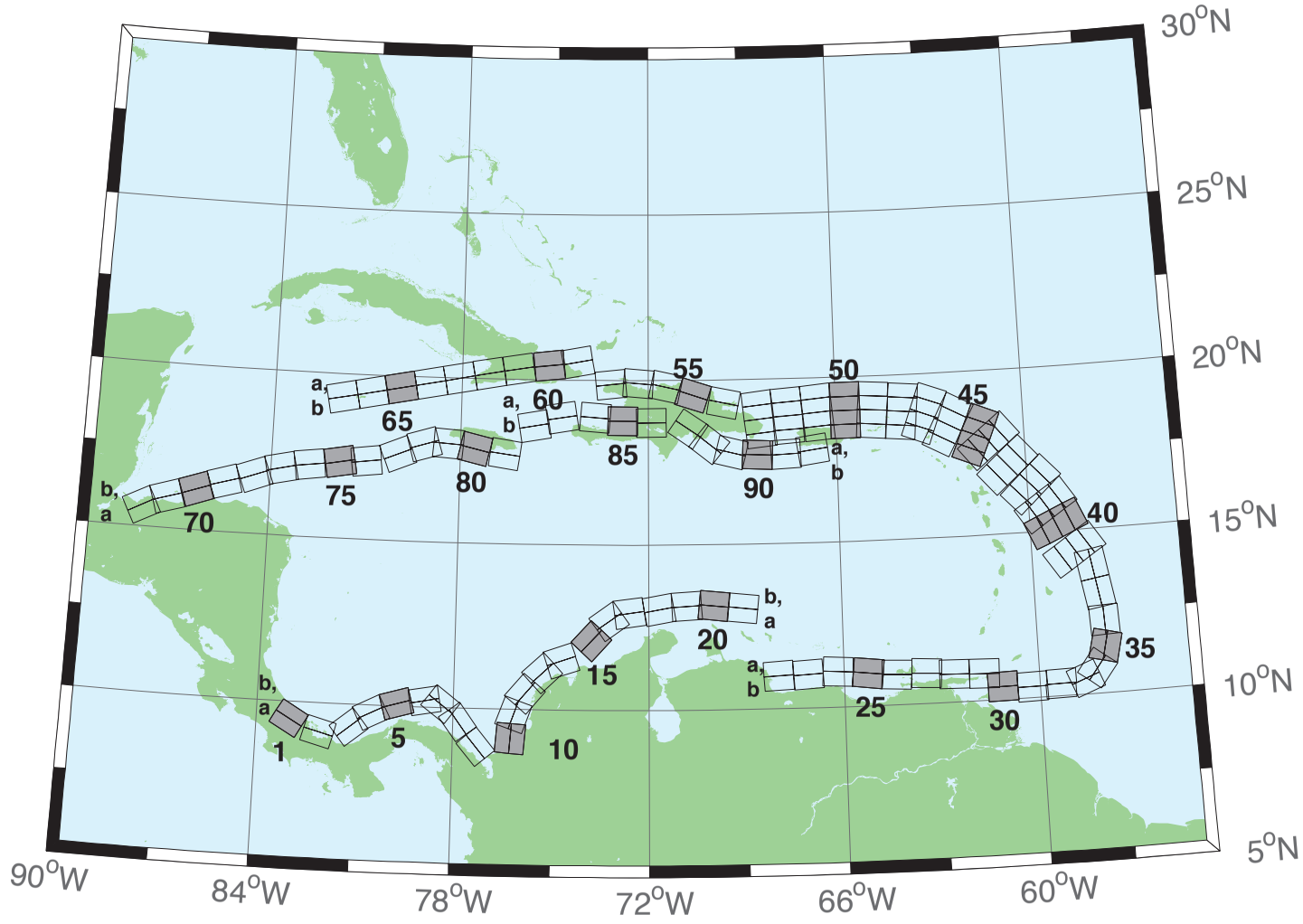

Figure B.1: Atlantic Source Zone unit sources.

Table B.1: Earthquake parameters for Atlantic Source Zone unit sources.

Segment	Description	Longitude(°E)	Latitude(°N)	Strike(°)	Dip(°)	Depth (km)
atsz–1a	Atlantic Source Zone	-83.2020	9.1449	120	27.5	28.09
atsz–1b	Atlantic Source Zone	-83.0000	9.4899	120	27.5	5
atsz–2a	Atlantic Source Zone	-82.1932	8.7408	105.1	27.5	28.09
atsz–2b	Atlantic Source Zone	-82.0880	9.1254	105.1	27.5	5
atsz–3a	Atlantic Source Zone	-80.9172	9.0103	51.31	30	30
atsz–3b	Atlantic Source Zone	-81.1636	9.3139	51.31	30	5
atsz–4a	Atlantic Source Zone	-80.3265	9.4308	63.49	30	30
atsz–4b	Atlantic Source Zone	-80.5027	9.7789	63.49	30	5
atsz–5a	Atlantic Source Zone	-79.6247	9.6961	74.44	30	30
atsz–5b	Atlantic Source Zone	-79.7307	10.0708	74.44	30	5
atsz–6a	Atlantic Source Zone	-78.8069	9.8083	79.71	30	30
atsz–6b	Atlantic Source Zone	-78.8775	10.1910	79.71	30	5
atsz–7a	Atlantic Source Zone	-78.6237	9.7963	127.2	30	30
atsz–7b	Atlantic Source Zone	-78.3845	10.1059	127.2	30	5
atsz–8a	Atlantic Source Zone	-78.1693	9.3544	143.8	30	30
atsz–8b	Atlantic Source Zone	-77.8511	9.5844	143.8	30	5
atsz–9a	Atlantic Source Zone	-77.5913	8.5989	139.9	30	30
atsz–9b	Atlantic Source Zone	-77.2900	8.8493	139.9	30	5
atsz–10a	Atlantic Source Zone	-75.8109	9.0881	4.67	17	19.62
atsz–10b	Atlantic Source Zone	-76.2445	9.1231	4.67	17	5
atsz–11a	Atlantic Source Zone	-75.7406	9.6929	19.67	17	19.62
atsz–11b	Atlantic Source Zone	-76.1511	9.8375	19.67	17	5
atsz–12a	Atlantic Source Zone	-75.4763	10.2042	40.4	17	19.62
atsz–12b	Atlantic Source Zone	-75.8089	10.4826	40.4	17	5
atsz–13a	Atlantic Source Zone	-74.9914	10.7914	47.17	17	19.62
atsz–13b	Atlantic Source Zone	-75.2890	11.1064	47.17	17	5
atsz–14a	Atlantic Source Zone	-74.5666	11.0708	71.68	17	19.62
atsz–14b	Atlantic Source Zone	-74.7043	11.4786	71.68	17	5
atsz–15a	Atlantic Source Zone	-73.4576	11.8012	42.69	17	19.62
atsz–15b	Atlantic Source Zone	-73.7805	12.0924	42.69	17	5
atsz–16a	Atlantic Source Zone	-72.9788	12.3365	54.75	17	19.62
atsz–16b	Atlantic Source Zone	-73.2329	12.6873	54.75	17	5
atsz–17a	Atlantic Source Zone	-72.5454	12.5061	81.96	17	19.62
atsz–17b	Atlantic Source Zone	-72.6071	12.9314	81.96	17	5
atsz–18a	Atlantic Source Zone	-71.6045	12.6174	79.63	17	19.62
atsz–18b	Atlantic Source Zone	-71.6839	13.0399	79.63	17	5
atsz–19a	Atlantic Source Zone	-70.7970	12.7078	86.32	17	19.62
atsz–19b	Atlantic Source Zone	-70.8253	13.1364	86.32	17	5
atsz–20a	Atlantic Source Zone	-70.0246	12.7185	95.94	17	19.62
atsz–20b	Atlantic Source Zone	-69.9789	13.1457	95.94	17	5
atsz–21a	Atlantic Source Zone	-69.1244	12.6320	95.94	17	19.62
atsz–21b	Atlantic Source Zone	-69.0788	13.0592	95.94	17	5
atsz–22a	Atlantic Source Zone	-68.0338	11.4286	266.9	15	17.94
atsz–22b	Atlantic Source Zone	-68.0102	10.9954	266.9	15	5
atsz–23a	Atlantic Source Zone	-67.1246	11.4487	266.9	15	17.94
atsz–23b	Atlantic Source Zone	-67.1010	11.0155	266.9	15	5
atsz–24a	Atlantic Source Zone	-66.1656	11.5055	273.3	15	17.94
atsz–24b	Atlantic Source Zone	-66.1911	11.0724	273.3	15	5
atsz–25a	Atlantic Source Zone	-65.2126	11.4246	276.4	15	17.94
atsz–25b	Atlantic Source Zone	-65.2616	10.9934	276.4	15	5
atsz–26a	Atlantic Source Zone	-64.3641	11.3516	272.9	15	17.94
atsz–26b	Atlantic Source Zone	-64.3862	10.9183	272.9	15	5
atsz–27a	Atlantic Source Zone	-63.4472	11.3516	272.9	15	17.94
atsz–27b	Atlantic Source Zone	-63.4698	10.9183	272.9	15	5
atsz–28a	Atlantic Source Zone	-62.6104	11.2831	271.1	15	17.94
atsz–28b	Atlantic Source Zone	-62.6189	10.8493	271.1	15	5
atsz–29a	Atlantic Source Zone	-61.6826	11.2518	271.6	15	17.94
atsz–29b	Atlantic Source Zone	-61.6947	10.8181	271.6	15	5
atsz–30a	Atlantic Source Zone	-61.1569	10.8303	269	15	17.94
atsz–30b	Atlantic Source Zone	-61.1493	10.3965	269	15	5

Continued on next page

Table B.1 – continued from previous page

Segment	Description	Longitude(°E)	Latitude(°N)	Strike(°)	Dip(°)	Depth (km)
atsz–31a	Atlantic Source Zone	-60.2529	10.7739	269	15	17.94
atsz–31b	Atlantic Source Zone	-60.2453	10.3401	269	15	5
atsz–32a	Atlantic Source Zone	-59.3510	10.8123	269	15	17.94
atsz–32b	Atlantic Source Zone	-59.3734	10.3785	269	15	5
atsz–33a	Atlantic Source Zone	-58.7592	10.8785	248.6	15	17.94
atsz–33b	Atlantic Source Zone	-58.5984	10.4745	248.6	15	5
atsz–34a	Atlantic Source Zone	-58.5699	11.0330	217.2	15	17.94
atsz–34b	Atlantic Source Zone	-58.2179	10.7710	217.2	15	5
atsz–35a	Atlantic Source Zone	-58.3549	11.5300	193.7	15	17.94
atsz–35b	Atlantic Source Zone	-57.9248	11.4274	193.7	15	5
atsz–36a	Atlantic Source Zone	-58.3432	12.1858	177.7	15	17.94
atsz–36b	Atlantic Source Zone	-57.8997	12.2036	177.7	15	5
atsz–37a	Atlantic Source Zone	-58.4490	12.9725	170.7	15	17.94
atsz–37b	Atlantic Source Zone	-58.0095	13.0424	170.7	15	5
atsz–38a	Atlantic Source Zone	-58.6079	13.8503	170.2	15	17.94
atsz–38b	Atlantic Source Zone	-58.1674	13.9240	170.2	15	5
atsz–39a	Atlantic Source Zone	-58.6667	14.3915	146.8	15	17.94
atsz–39b	Atlantic Source Zone	-58.2913	14.6287	146.8	15	5
atsz–39y	Atlantic Source Zone	-59.4168	13.9171	146.8	15	43.82
atsz–39z	Atlantic Source Zone	-59.0415	14.1543	146.8	15	30.88
atsz–40a	Atlantic Source Zone	-59.1899	15.2143	156.2	15	17.94
atsz–40b	Atlantic Source Zone	-58.7781	15.3892	156.2	15	5
atsz–40y	Atlantic Source Zone	-60.0131	14.8646	156.2	15	43.82
atsz–40z	Atlantic Source Zone	-59.6012	15.0395	156.2	15	30.88
atsz–41a	Atlantic Source Zone	-59.4723	15.7987	146.3	15	17.94
atsz–41b	Atlantic Source Zone	-59.0966	16.0392	146.3	15	5
atsz–41y	Atlantic Source Zone	-60.2229	15.3177	146.3	15	43.82
atsz–41z	Atlantic Source Zone	-59.8473	15.5582	146.3	15	30.88
atsz–42a	Atlantic Source Zone	-59.9029	16.4535	137	15	17.94
atsz–42b	Atlantic Source Zone	-59.5716	16.7494	137	15	5
atsz–42y	Atlantic Source Zone	-60.5645	15.8616	137	15	43.82
atsz–42z	Atlantic Source Zone	-60.2334	16.1575	137	15	30.88
atsz–43a	Atlantic Source Zone	-60.5996	17.0903	138.7	15	17.94
atsz–43b	Atlantic Source Zone	-60.2580	17.3766	138.7	15	5
atsz–43y	Atlantic Source Zone	-61.2818	16.5177	138.7	15	43.82
atsz–43z	Atlantic Source Zone	-60.9404	16.8040	138.7	15	30.88
atsz–44a	Atlantic Source Zone	-61.1559	17.8560	141.1	15	17.94
atsz–44b	Atlantic Source Zone	-60.8008	18.1286	141.1	15	5
atsz–44y	Atlantic Source Zone	-61.8651	17.3108	141.1	15	43.82
atsz–44z	Atlantic Source Zone	-61.5102	17.5834	141.1	15	30.88
atsz–45a	Atlantic Source Zone	-61.5491	18.0566	112.8	15	17.94
atsz–45b	Atlantic Source Zone	-61.3716	18.4564	112.8	15	5
atsz–45y	Atlantic Source Zone	-61.9037	17.2569	112.8	15	43.82
atsz–45z	Atlantic Source Zone	-61.7260	17.6567	112.8	15	30.88
atsz–46a	Atlantic Source Zone	-62.4217	18.4149	117.9	15	17.94
atsz–46b	Atlantic Source Zone	-62.2075	18.7985	117.9	15	5
atsz–46y	Atlantic Source Zone	-62.8493	17.6477	117.9	15	43.82
atsz–46z	Atlantic Source Zone	-62.6352	18.0313	117.9	15	30.88
atsz–47a	Atlantic Source Zone	-63.1649	18.7844	110.5	20	22.1
atsz–47b	Atlantic Source Zone	-63.0087	19.1798	110.5	20	5
atsz–47y	Atlantic Source Zone	-63.4770	17.9936	110.5	20	56.3
atsz–47z	Atlantic Source Zone	-63.3205	18.3890	110.5	20	39.2
atsz–48a	Atlantic Source Zone	-63.8800	18.8870	95.37	20	22.1
atsz–48b	Atlantic Source Zone	-63.8382	19.3072	95.37	20	5
atsz–48y	Atlantic Source Zone	-63.9643	18.0465	95.37	20	56.3
atsz–48z	Atlantic Source Zone	-63.9216	18.4667	95.37	20	39.2
atsz–49a	Atlantic Source Zone	-64.8153	18.9650	94.34	20	22.1
atsz–49b	Atlantic Source Zone	-64.7814	19.3859	94.34	20	5
atsz–49y	Atlantic Source Zone	-64.8840	18.1233	94.34	20	56.3
atsz–49z	Atlantic Source Zone	-64.8492	18.5442	94.34	20	39.2
atsz–50a	Atlantic Source Zone	-65.6921	18.9848	89.59	20	22.1

Continued on next page

Table B.1 – continued from previous page

Segment	Description	Longitude(°E)	Latitude(°N)	Strike(°)	Dip(°)	Depth (km)
atsz–50b	Atlantic Source Zone	-65.6953	19.4069	89.59	20	5
atsz–50y	Atlantic Source Zone	-65.6874	18.1407	89.59	20	56.3
atsz–50z	Atlantic Source Zone	-65.6887	18.5628	89.59	20	39.2
atsz–51a	Atlantic Source Zone	-66.5742	18.9484	84.98	20	22.1
atsz–51b	Atlantic Source Zone	-66.6133	19.3688	84.98	20	5
atsz–51y	Atlantic Source Zone	-66.4977	18.1076	84.98	20	56.3
atsz–51z	Atlantic Source Zone	-66.5353	18.5280	84.98	20	39.2
atsz–52a	Atlantic Source Zone	-67.5412	18.8738	85.87	20	22.1
atsz–52b	Atlantic Source Zone	-67.5734	19.2948	85.87	20	5
atsz–52y	Atlantic Source Zone	-67.4781	18.0319	85.87	20	56.3
atsz–52z	Atlantic Source Zone	-67.5090	18.4529	85.87	20	39.2
atsz–53a	Atlantic Source Zone	-68.4547	18.7853	83.64	20	22.1
atsz–53b	Atlantic Source Zone	-68.5042	19.2048	83.64	20	5
atsz–53y	Atlantic Source Zone	-68.3575	17.9463	83.64	20	56.3
atsz–53z	Atlantic Source Zone	-68.4055	18.3658	83.64	20	39.2
atsz–54a	Atlantic Source Zone	-69.6740	18.8841	101.5	20	22.1
atsz–54b	Atlantic Source Zone	-69.5846	19.2976	101.5	20	5
atsz–55a	Atlantic Source Zone	-70.7045	19.1376	108.2	20	22.1
atsz–55b	Atlantic Source Zone	-70.5647	19.5386	108.2	20	5
atsz–56a	Atlantic Source Zone	-71.5368	19.3853	102.6	20	22.1
atsz–56b	Atlantic Source Zone	-71.4386	19.7971	102.6	20	5
atsz–57a	Atlantic Source Zone	-72.3535	19.4838	94.2	20	22.1
atsz–57b	Atlantic Source Zone	-72.3206	19.9047	94.2	20	5
atsz–58a	Atlantic Source Zone	-73.1580	19.4498	84.34	20	22.1
atsz–58b	Atlantic Source Zone	-73.2022	19.8698	84.34	20	5
atsz–59a	Atlantic Source Zone	-74.3567	20.9620	259.7	20	22.1
atsz–59b	Atlantic Source Zone	-74.2764	20.5467	259.7	20	5
atsz–60a	Atlantic Source Zone	-75.2386	20.8622	264.2	15	17.94
atsz–60b	Atlantic Source Zone	-75.1917	20.4306	264.2	15	5
atsz–61a	Atlantic Source Zone	-76.2383	20.7425	260.7	15	17.94
atsz–61b	Atlantic Source Zone	-76.1635	20.3144	260.7	15	5
atsz–62a	Atlantic Source Zone	-77.2021	20.5910	259.9	15	17.94
atsz–62b	Atlantic Source Zone	-77.1214	20.1638	259.9	15	5
atsz–63a	Atlantic Source Zone	-78.1540	20.4189	259	15	17.94
atsz–63b	Atlantic Source Zone	-78.0661	19.9930	259	15	5
atsz–64a	Atlantic Source Zone	-79.0959	20.2498	259.2	15	17.94
atsz–64b	Atlantic Source Zone	-79.0098	19.8236	259.2	15	5
atsz–65a	Atlantic Source Zone	-80.0393	20.0773	258.9	15	17.94
atsz–65b	Atlantic Source Zone	-79.9502	19.6516	258.9	15	5
atsz–66a	Atlantic Source Zone	-80.9675	19.8993	258.6	15	17.94
atsz–66b	Atlantic Source Zone	-80.8766	19.4740	258.6	15	5
atsz–67a	Atlantic Source Zone	-81.9065	19.7214	258.5	15	17.94
atsz–67b	Atlantic Source Zone	-81.8149	19.2962	258.5	15	5
atsz–68a	Atlantic Source Zone	-87.8003	15.2509	62.69	15	17.94
atsz–68b	Atlantic Source Zone	-88.0070	15.6364	62.69	15	5
atsz–69a	Atlantic Source Zone	-87.0824	15.5331	72.73	15	17.94
atsz–69b	Atlantic Source Zone	-87.2163	15.9474	72.73	15	5
atsz–70a	Atlantic Source Zone	-86.1622	15.8274	70.64	15	17.94
atsz–70b	Atlantic Source Zone	-86.3120	16.2367	70.64	15	5
atsz–71a	Atlantic Source Zone	-85.3117	16.1052	73.7	15	17.94
atsz–71b	Atlantic Source Zone	-85.4387	16.5216	73.7	15	5
atsz–72a	Atlantic Source Zone	-84.3470	16.3820	69.66	15	17.94
atsz–72b	Atlantic Source Zone	-84.5045	16.7888	69.66	15	5
atsz–73a	Atlantic Source Zone	-83.5657	16.6196	77.36	15	17.94
atsz–73b	Atlantic Source Zone	-83.6650	17.0429	77.36	15	5
atsz–74a	Atlantic Source Zone	-82.7104	16.7695	82.35	15	17.94
atsz–74b	Atlantic Source Zone	-82.7709	17.1995	82.35	15	5
atsz–75a	Atlantic Source Zone	-81.7297	16.9003	79.86	15	17.94
atsz–75b	Atlantic Source Zone	-81.8097	17.3274	79.86	15	5
atsz–76a	Atlantic Source Zone	-80.9196	16.9495	82.95	15	17.94
atsz–76b	Atlantic Source Zone	-80.9754	17.3801	82.95	15	5

Continued on next page

Table B.1 – continued from previous page

Segment	Description	Longitude(°E)	Latitude(°N)	Strike(°)	Dip(°)	Depth (km)
atsz–77a	Atlantic Source Zone	-79.8086	17.2357	67.95	15	17.94
atsz–77b	Atlantic Source Zone	-79.9795	17.6378	67.95	15	5
atsz–78a	Atlantic Source Zone	-79.0245	17.5415	73.61	15	17.94
atsz–78b	Atlantic Source Zone	-79.1532	17.9577	73.61	15	5
atsz–79a	Atlantic Source Zone	-78.4122	17.5689	94.07	15	17.94
atsz–79b	Atlantic Source Zone	-78.3798	18.0017	94.07	15	5
atsz–80a	Atlantic Source Zone	-77.6403	17.4391	103.3	15	17.94
atsz–80b	Atlantic Source Zone	-77.5352	17.8613	103.3	15	5
atsz–81a	Atlantic Source Zone	-76.6376	17.2984	98.21	15	17.94
atsz–81b	Atlantic Source Zone	-76.5726	17.7278	98.21	15	5
atsz–82a	Atlantic Source Zone	-75.7299	19.0217	260.1	15	17.94
atsz–82b	Atlantic Source Zone	-75.6516	18.5942	260.1	15	5
atsz–83a	Atlantic Source Zone	-74.8351	19.2911	260.8	15	17.94
atsz–83b	Atlantic Source Zone	-74.7621	18.8628	260.8	15	5
atsz–84a	Atlantic Source Zone	-73.6639	19.2991	274.8	15	17.94
atsz–84b	Atlantic Source Zone	-73.7026	18.8668	274.8	15	5
atsz–85a	Atlantic Source Zone	-72.8198	19.2019	270.6	15	17.94
atsz–85b	Atlantic Source Zone	-72.8246	18.7681	270.6	15	5
atsz–86a	Atlantic Source Zone	-71.9143	19.1477	269.1	15	17.94
atsz–86b	Atlantic Source Zone	-71.9068	18.7139	269.1	15	5
atsz–87a	Atlantic Source Zone	-70.4738	18.8821	304.5	15	17.94
atsz–87b	Atlantic Source Zone	-70.7329	18.5245	304.5	15	5
atsz–88a	Atlantic Source Zone	-69.7710	18.3902	308.9	15	17.94
atsz–88b	Atlantic Source Zone	-70.0547	18.0504	308.4	15	5
atsz–89a	Atlantic Source Zone	-69.2635	18.2099	283.9	15	17.94
atsz–89b	Atlantic Source Zone	-69.3728	17.7887	283.9	15	5
atsz–90a	Atlantic Source Zone	-68.5059	18.1443	272.9	15	17.94
atsz–90b	Atlantic Source Zone	-68.5284	17.7110	272.9	15	5
atsz–91a	Atlantic Source Zone	-67.6428	18.1438	267.8	15	17.94
atsz–91b	Atlantic Source Zone	-67.6256	17.7103	267.8	15	5
atsz–92a	Atlantic Source Zone	-66.8261	18.2536	262	15	17.94
atsz–92b	Atlantic Source Zone	-66.7627	17.8240	262	15	5

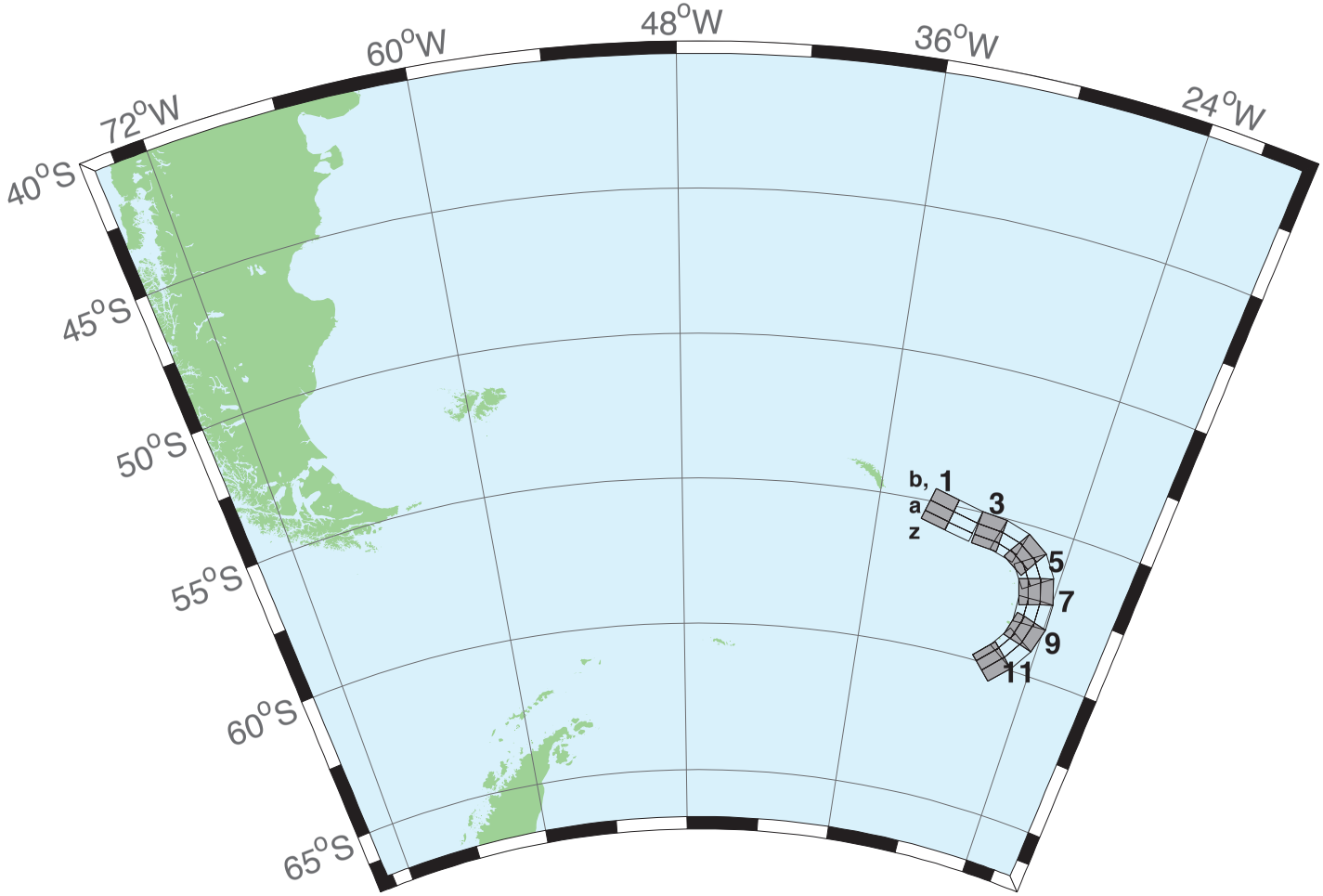

Figure B.2: South Sandwich Islands Subduction Zone.

Table B.2: Earthquake parameters for South Sandwich Islands Subduction Zone unit sources.

Segment	Description	Longitude(°E)	Latitude(°N)	Strike(°)	Dip(°)	Depth (km)
sssz–1a	South Sandwich Islands Subduction Zone	-32.3713	-55.4655	104.7	28.53	17.51
sssz–1b	South Sandwich Islands Subduction Zone	-32.1953	-55.0832	104.7	9.957	8.866
sssz–1z	South Sandwich Islands Subduction Zone	-32.5091	-55.7624	104.7	46.99	41.39
sssz–2a	South Sandwich Islands Subduction Zone	-30.8028	-55.6842	102.4	28.53	17.51
sssz–2b	South Sandwich Islands Subduction Zone	-30.6524	-55.2982	102.4	9.957	8.866
sssz–2z	South Sandwich Islands Subduction Zone	-30.9206	-55.9839	102.4	46.99	41.39
sssz–3a	South Sandwich Islands Subduction Zone	-29.0824	-55.8403	95.53	28.53	17.51
sssz–3b	South Sandwich Islands Subduction Zone	-29.0149	-55.4468	95.53	9.957	8.866
sssz–3z	South Sandwich Islands Subduction Zone	-29.1353	-56.1458	95.53	46.99	41.39
sssz–4a	South Sandwich Islands Subduction Zone	-27.8128	-55.9796	106.1	28.53	17.51
sssz–4b	South Sandwich Islands Subduction Zone	-27.6174	-55.5999	106.1	9.957	8.866
sssz–4z	South Sandwich Islands Subduction Zone	-27.9659	-56.2744	106.1	46.99	41.39
sssz–5a	South Sandwich Islands Subduction Zone	-26.7928	-56.2481	123.1	28.53	17.51
sssz–5b	South Sandwich Islands Subduction Zone	-26.4059	-55.9170	123.1	9.957	8.866
sssz–5z	South Sandwich Islands Subduction Zone	-27.0955	-56.5052	123.1	46.99	41.39
sssz–6a	South Sandwich Islands Subduction Zone	-26.1317	-56.6466	145.6	23.28	16.11
sssz–6b	South Sandwich Islands Subduction Zone	-25.5131	-56.4133	145.6	9.09	8.228
sssz–6z	South Sandwich Islands Subduction Zone	-26.5920	-56.8194	145.6	47.15	35.87
sssz–7a	South Sandwich Islands Subduction Zone	-25.6787	-57.2162	162.9	21.21	14.23
sssz–7b	South Sandwich Islands Subduction Zone	-24.9394	-57.0932	162.9	7.596	7.626
sssz–7z	South Sandwich Islands Subduction Zone	-26.2493	-57.3109	162.9	44.16	32.32
sssz–8a	South Sandwich Islands Subduction Zone	-25.5161	-57.8712	178.2	20.33	15.91
sssz–8b	South Sandwich Islands Subduction Zone	-24.7233	-57.8580	178.2	8.449	8.562
sssz–8z	South Sandwich Islands Subduction Zone	-26.1280	-57.8813	178.2	43.65	33.28
sssz–9a	South Sandwich Islands Subduction Zone	-25.6657	-58.5053	195.4	25.76	15.71
sssz–9b	South Sandwich Islands Subduction Zone	-24.9168	-58.6127	195.4	8.254	8.537
sssz–9z	South Sandwich Islands Subduction Zone	-26.1799	-58.4313	195.4	51.69	37.44
sssz–10a	South Sandwich Islands Subduction Zone	-26.1563	-59.1048	212.5	32.82	15.65
sssz–10b	South Sandwich Islands Subduction Zone	-25.5335	-59.3080	212.5	10.45	6.581
sssz–10z	South Sandwich Islands Subduction Zone	-26.5817	-58.9653	212.5	54.77	42.75
sssz–11a	South Sandwich Islands Subduction Zone	-27.0794	-59.6799	224.2	33.67	15.75
sssz–11b	South Sandwich Islands Subduction Zone	-26.5460	-59.9412	224.2	11.32	5.927
sssz–11z	South Sandwich Islands Subduction Zone	-27.4245	-59.5098	224.2	57.19	43.46

Appendix C

SIFT Testing

Authors: Burak Uslu, Lindsey Wright

C.1 Purpose

Forecast models are tested with synthetic tsunami events covering a range of tsunami source locations and magnitudes. Testing is also done with selected historical tsunami events when available.

The purpose of forecast model testing is three-fold. The first objective is to assure that the results obtained with the NOAA's tsunami forecast system software, which has been released to the Tsunami Warning Centers for operational use, are consistent with those obtained by the researcher during the development of the forecast model. The second objective is to test the forecast model for consistency, accuracy, time efficiency, and quality of results over a range of possible tsunami locations and magnitudes. The third objective is to identify bugs and issues in need of resolution by the researcher who developed the Forecast Model or by the forecast system software development team before the next version release to NOAA's two Tsunami Warning Centers.

Local hardware and software applications, and tools familiar to the researcher(s), are used to run the Method of Splitting Tsunamis (MOST) model during the forecast model development. The test results presented in this report lend confidence that the model performs as developed and produces the same results when initiated within the forecast system application in an operational setting as those produced by the researcher during the forecast model development. The test results assure those who rely on the Savannah tsunami forecast model that consistent results are produced irrespective of system.

C.2 Testing Procedure

The general procedure for forecast model testing is to run a set of synthetic tsunami scenarios and a selected set of historical tsunami events through the forecast system application and compare the results with those obtained by the researcher during the forecast model development and presented in the Tsunami Forecast Model Report. Specific steps taken to test the model include:

1. Identification of testing scenarios, including the standard set of synthetic events, appropriate historical events, and customized synthetic scenarios that may have been used by the researcher(s) in developing the forecast model.
2. Creation of new events to represent customized synthetic scenarios used by the researcher(s) in developing the forecast model, if any.
3. Submission of test model runs with the forecast system, and export of the results from A, B, and C grids, along with time series.
4. Recording applicable metadata, including the specific version used for testing.
5. Examination of forecast system model results for instabilities in both time series and plot results.
6. Comparison of forecast model results obtained through the forecast system with those obtained during the forecast model development.
7. Summarization of results with specific mention of quality, consistency, and time efficiency.
8. Reporting of issues identified to modeler and forecast software development team.
9. Retesting the forecast models in the forecast system when reported issues have been addressed or explained.

Synthetic model runs were tested on a DELL PowerEdge R510 computer equipped with two Xeon E5670 processors at 2.93 Ghz, each with 12 MBytes of cache and 32GB memory. The processors are hex core and support hyperthreading, resulting in the computer performing as a 24 processor core machine. Additionally, the testing computer supports 10 Gigabit Ethernet for fast network connections. This computer configuration is similar or the same as the configurations of the computers installed at the Tsunami Warning Centers so the compute times should only vary slightly.

C.3 Results

The Mayaguez forecast model was tested with SIFT version 3.2.

The Mayaguez, Puerto Rico forecast model was tested with three synthetic scenarios. Test results from the forecast system and comparisons with the results obtained during the forecast model development are shown numerically in Table C.1 and graphically in Figures C.1,C.2 and C.3. The results show that the minimum and maximum amplitudes and time series obtained from the forecast system agree with those obtained during the forecast model development, and that the forecast model is stable and robust, with consistent and high quality results across geographically distributed tsunami sources. The model run time (wall clock time) was 12.55 minutes for 10 hours of simulation time, and 5.0 minutes for 4.0 hours. This run time is within the 10 minute run time for 4 hours of simulation time and satisfies run time requirements.

A suite of three synthetic events was run on the Mayaguez forecast model. The modeled scenarios were stable for all cases run. Amplitudes of less than 75 centimeters (cm) were observed for all cases tested. The largest modeled height was 818.9 cm from the Atlantic (ATSZ

48-57) source zone. The smallest signal of 31.4 cm was recorded at the far field South Sandwich (SSSZ 1-10) source zone. The comparisons between the development cases and the forecast system output were consistent in shape and amplitude for all three cases. The Mayaguez reference point used for the forecast model development is the same as what is deployed in the forecast system, so the results can be considered valid for the three cases studied.

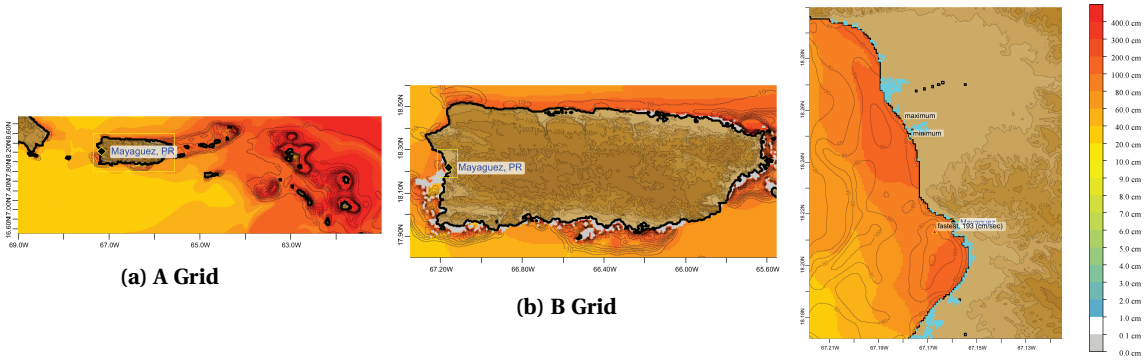

(a) A Grid

(b) B Grid

(c) C Grid

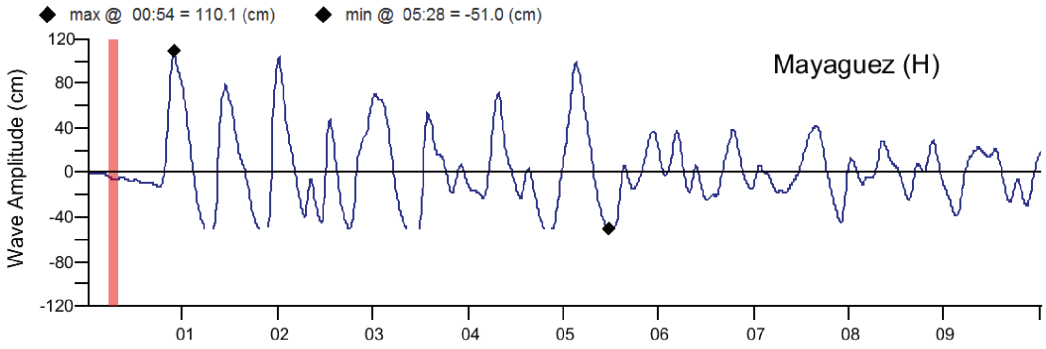

(d)

Figure C.1: Response of the Mayaguez forecast model to synthetic scenario ATSZ 38-47 (alpha=25). Maximum sea surface elevation for (a) A-grid, b) B-grid, c) C-grid. Sea surface elevation time series at the C-grid warning point (d) The lower time series plot is the result obtained during model development and is shown for comparison with test results.

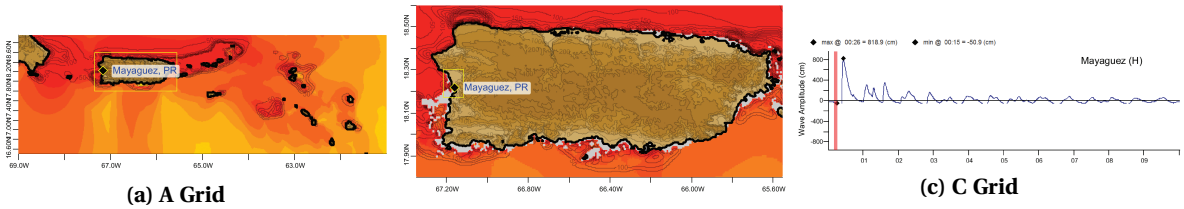

(a) A Grid

(b) B Grid

(c) C Grid

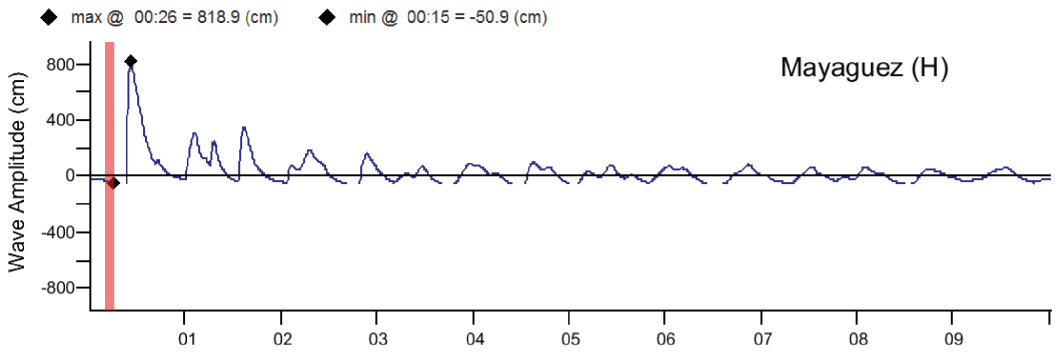

(d)

Figure C.2: Response of the Mayaguez forecast model to synthetic scenario ATSZ 48-57 (alpha=25). Maximum sea surface elevation for (a) A-grid, b) B-grid, c) C-grid. Sea surface elevation time series at the C-grid warning point (d) The lower time series plot is the result obtained during model development and is shown for comparison with test results.

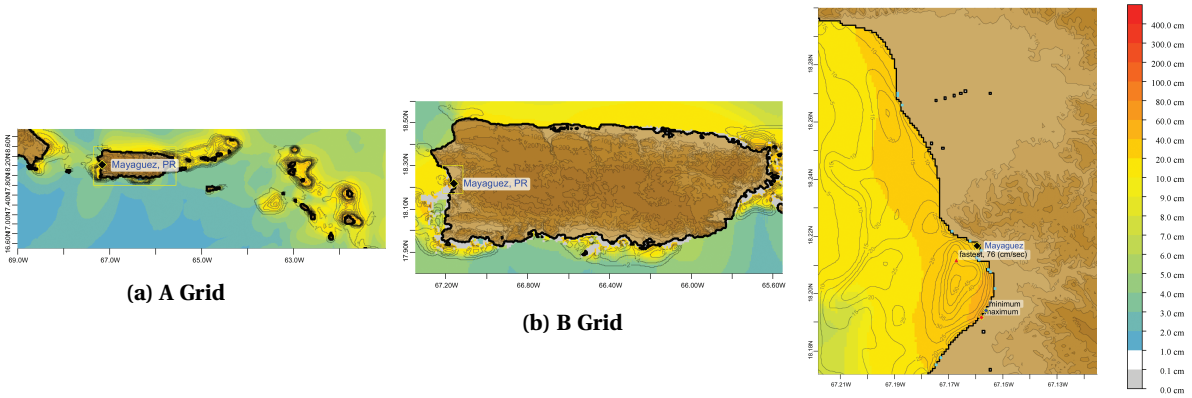

(a) A Grid

(b) B Grid

(c) C Grid

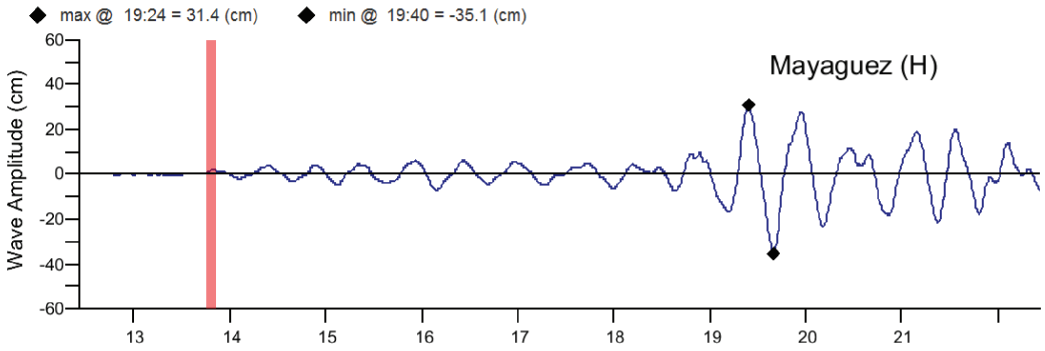

(d)

Figure C.3: Response of the Mayaguez forecast model to synthetic scenario SSSZ 1-10 (alpha=25). Maximum sea surface elevation for (a) A-grid, b) B-grid, c) C-grid. Sea surface elevation time series at the C-grid warning point (d) The lower time series plot is the result obtained during model development and is shown for comparison with test results.

Table C.1: Table of maximum and minimum amplitudes (cm) at the Mayaguez, Puerto Rico warning point for synthetic and historical events tested using SIFT 3.2 and obtained during development.

Scenario Name	Source Zone	Tsunami Source	α (m)	SIFT Max (cm)	Development Max (cm)	SIFT Min (cm)	Development Min (cm)
Mega-tsunami Scenarios							
ATSZ 35-44	Atlantic	A38-A47, B38-B47	25	110.1	110.1	-51.0	-51.0
ATSZ 48-57	Atlantic	A48-A57, B48-B57	25	818.9	818.95	-50.9	-50.93
SSSZ 1-10	South Sandwich	A1-A10, B1-B10	25	31.4	31.41	-35.1	-35.09

Glossary

Arrival time The time when the first tsunami wave is observed at a particular location, typically given in local and/or universal time, but also commonly noted in minutes or hours relative to the time of the earthquake.

Bathymetry The measurement of water depth of an undisturbed body of water.

Cascadia Subduction Zone Fault that extends from Cape Mendocino in Northern California northward to mid-Vancouver Island Canada. The fault marks the convergence boundary where the Juan de Fuca tectonic plate is being subducted under the margin of the North America plate.

Current speed The scalar rate of water motion measured as distance/time.

Current velocity Movement of water expressed as a vector quantity. Velocity is the distance of movement per time coupled with direction of motion.

Digital Elevation Model (DEM) A digital representation of bathymetry or topography based on regional survey data or satellite imagery. Data are arrays of regularly spaced elevations referenced to a map projection of the geographic coordinate system.

Epicenter The point on the surface of the earth that is directly above the focus of an earthquake.

Focus The point beneath the surface of the earth where a rupture or energy release occurs due to a buildup of stress or the movement of earth's tectonic plates relative to one another.

Inundation The horizontal inland extent of land that a tsunami penetrates, generally measured perpendicularly to a shoreline.

Marigram Tide gauge recording of wave level as a function of time at a particular location. The instrument used for recording is termed a marigraph.

Moment Magnitude (M_W) The magnitude of an earthquake on a logarithmic scale in terms of the energy released. Moment magnitude is based on the size and characteristics of a fault rupture as determined from long-period seismic waves.

Method of Splitting Tsunamis (MOST) A suite of numerical simulation codes used to provide estimates of the three processes of tsunami evolution: tsunami generation, propagation, and inundation.

Near–field A particular location at which the earth's deformation due to energy release affects the modeling solution.

Propagation database A basin-wide database of pre-computed water elevations and flow velocities at uniformly spaced grid points throughout the world oceans. Values are computed from tsunamis generated by earthquakes with a fault rupture at any one of discrete 100 × 50 km unit sources along worldwide subduction zones.

Runup Vertical difference between the elevation of tsunami inundation and the sea level at the time of a tsunami. Runup is the elevation of the highest point of land inundated by a tsunami as measured relative to a stated datum, such as mean sea level.

Short-term Inundation Forecasting for Tsunamis (SIFT) A tsunami forecast system that integrates tsunami observations in the deep-ocean with numerical models to provide an estimate of tsunami wave arrival and amplitude at specific coastal locations while a tsunami propagates across an ocean basin.

Subduction zone A submarine region of the earth's crust at which two or more tectonic plates converge to cause one plate to sink under another, overriding plate. Subduction zones are regions of high seismic activity.

Synthetic event Hypothetical events based on computer simulations or theory of possible or even likely future scenarios.

Tidal wave Term frequently used incorrectly as a synonym for tsunami. A tsunami is unrelated to the predictable periodic rise and fall of sea level due to the gravitational attractions of the moon and sun: the tide.

Tide The predictable rise and fall of a body of water (ocean, sea, bay, etc.) due to the gravitational attractions of the moon and sun.

Tide gauge An instrument for measuring the rise and fall of a column of water over time at a particular location.

Tele–tsunami or distant tsunami or far–field tsunami Most commonly, a tsunami originating from a source greater than 1000 km away from a particular location. In some contexts, a tele-tsunami is one that propagates through deep-ocean before reaching a particular location without regard to distance separation.

Travel time The time it takes for a tsunami to travel from the generating source to a particular location.

tsunami A Japanese term that literally translates to "harbor wave." Tsunamis are a series of long–period shallow water waves that are generated by the sudden displacement of water due to subsea disturbances such as earthquakes, submarine landslides, or volcanic eruptions. Less commonly, meteoric impact to the ocean or meteorological forcing can generate a tsunami.

Tsunami Hazard Assessment A systematic investigation of seismically active regions of the world oceans to determine their potential tsunami impact at a particular location. Numerical models are typically used to characterize tsunami generation, propagation, and inundation, and to quantify the risk posed to a particular community from tsunamis generated in each source region investigated.

Tsunami Propagation The directional movement of a tsunami wave outward from the source of generation. The speed at which a tsunami propagates depends on the depth of the water column in which the wave is traveling. Tsunamis travel at a speed of 700 km/hr (450 mi/hr) over the average depth of 4000 m in the open deep Pacific Ocean.

Tsunami source Location of tsunami origin, most typically an underwater earthquake epicenter. Tsunamis are also generated by submarine landslides, underwater volcanic eruptions, or, less commonly, by meteoric impact of the ocean.

Wave amplitude The maximum vertical rise or drop of a column of water as measured from wave crest (peak) or trough to a defined mean water level state.

Wave crest or peak The highest part of a wave or maximum rise above a defined mean water level state, such as mean lower low water.

Wave height The vertical difference between the highest part of a specific wave (crest) and it's corresponding lowest point (trough).

Wavelength The horizontal distance between two successive wave crests or troughs.

Wave period The length of time between the passage of two successive wave crests or troughs as measured at a fixed location.

Wave trough The lowest part of a wave or the maximum drop below a defined mean water level state, such as mean lower low water.